Elucidating mechanisms in haem copper oxidases: The high-affinity Q_H binding site in quinol oxidase as studied by DONUT-HYSCORE spectroscopy and density functional theory

Fraser MacMillan,*[a] Sylwia Kacprzak,[b] Petra Hellwig,[c] Stephane Grimaldi,[d] Hartmut Michel[e] and Martin Kaupp*[f]

Received 20th April 2010, Accepted 18th May 2010
DOI: 10.1039/c005149g

The Cytochrome bo_3 ubiquinol oxidase (QOX) from *Escherichia coli* (*E. coli*) contains a redox-active quinone, the so-called "high-affinity" Q_H quinone. The location of this cofactor and its binding site has yet to be accurately determined by X-ray crystallographic studies. Based on site-directed mutagenesis studies, a putative quinone binding site in the protein has been proposed. The exact binding partner of this cofactor and also whether it is stabilised as an anionic semiquinone or as a neutral radical species is a matter of some speculation. Both Hyperfine Sub-level Correlation (HYSCORE) and Double Nuclear Coherence Transfer Spectroscopy (DONUT-HYSCORE) spectroscopy as well as density functional theory (DFT) have been applied to investigate the Q_H binding site in detail to resolve these issues. Use is made of site-directed variants as well as globally $^{15}N/^{14}N$-exchanged protein. Comparison of computed and experimental ^{13}C hyperfine tensors provides strong support for the binding of the semiquinone radical in an anionic rather than a neutral protonated form. These results are compared with the corresponding information available on other protein binding sites and/or on model systems and are discussed with regard to the location and potential function of Q_H in the overall mechanism of function of this family of haem copper oxidases.

Introduction

The cytochrome bo_3 ubiquinol oxidase (QOX) from *Escherichia coli* (*E. coli*) is a transmembrane protein belonging to the family of terminal copper-heme oxidases of the aerobic respiratory chain and acts as a redox-driven proton pump that couples the vectorial translocation of protons across the membrane to the reduction of molecular oxygen to water.[1–3] It catalyses both the two-electron oxidation of ubiquinol-8 (UQ_8) and the four-electron reduction of dioxygen. The presence of up to

[a]*Henry Wellcome Unit of Biological EPR, School of Chemistry, University of East Anglia, Norwich, NR4 7TJ, UK. E-mail: fraser.macmillan@uea.ac.uk*
[b]*Institut für Physikalische Chemie, Universität Freiburg, D-79104 Freiburg, Germany*
[c]*Institut de Chimie, UMR 7177, Université de Strasbourg, Strasbourg, F-67000, France*
[d]*Université d'Aix-Marseille/CNRS, BIP UPR 9036, F-13402 Marseille, France*
[e]*Max-Planck Institut für Biophysik, D-60437 Frankfurt am Main, Germany*
[f]*Technische Universität Berlin, Institut für Chemie, Sekr. C7, Strasse des 17. Juni 135, D-10623 Berlin, Germany*

two UQ_8 binding sites with distinct functional roles has been discussed for QOX over the last few years.[3] In one possible mechanism, ubiquinone bound at a high affinity site, acting as a cofactor, mediates electron transfer from the ubiquinol substrate, which binds to a low-affinity binding-site, to the low-spin haem *b*.[3–6] The electrons needed for the reduction process are derived from a membrane-soluble UQ_8 cofactor bound to this low affinity binding-site (Q_L) of QOX and transferred to the next electron acceptor (haem *b*) *via* the second so-called high affinity (Q_H) binding-site. The quinone cofactor tightly bound at the Q_H site changes its redox states between a fully oxidised and a doubly reduced quinone and has been suggested to act as a redox mediator between the two-electron oxidation of the quinol pool and the sequential one-electron transfer processes involved in reduction of oxygen at the heme-copper binuclear centre. This has been supported by studies which show that the Q_H site stabilises a semiquinone form of the cofactor. Reduced haem *b* then provides electrons to the haem-copper binuclear centre, formed by haem o_3 and Cu_B, where dioxygen binds and is reduced to water. The location of the two proposed quinone-binding sites within QOX is not clear and, indeed, direct unambiguous evidence that there are two different sites is lacking.[6–9] In contrast to the deduced low-affinity quinol binding site, the presence of a tightly bound quinone has become clearer.

This tightly bound quinone can be isolated with the purified enzyme and, significantly, forms a stabilised ubisemiquinone radical, which has been implicated as an intermediate during enzyme turnover.[10–13] The semiquinone radical has been examined in detail by continuous wave (cw-) electron paramagnetic resonance (EPR), electron nuclear double resonance (ENDOR) and more recently by electron spin-echo envelope modulation (ESEEM) spectroscopy, which indicate binding to the protein *via* direct hydrogen bonding to an amino acid residue.[11,14–18]

The crystal structure of cytochrome bo_3 from *E. coli* has been solved to approximately 3.5 Å resolution and while a quinone moiety could not be resolved in this model of the enzyme, amino acids forming a putative binding motif able to bind ubiquinone were recognised[19] and a quinone binding-site within subunit I was postulated based on the X-ray data. In the model (see Fig. 1) Q101 and H98 were proposed to interact with ubiquinone at the C_4=O moiety, whereas D75 and R71 were proposed as hydrogen bond partners to the C_1=O moiety of the bound ubiquinone. This binding site is located in subunit I close to haem *b* in a position analogous to Cu_A in *e.g.* cytochrome *c* oxidase from *Paracoccus denitrificans*.[20] Site-directed mutagenesis has provided support for this model, insofar as several variants result in strongly reduced quinol oxidase activity and increased K_m values for quinol oxidation.[19] A combined cw-EPR spectroscopic and site-directed mutagenesis approach demonstrated that H98 and R71 are crucial residues for the high-affinity binding site of QOX, and are required for stabilisation of the semiquinone radical formed during catalytic turnover, whereas mutants at I102, Q101 and D75 did not directly affect the radical stabilisation.[21] Electrochemically-induced FTIR difference spectra of the D75E mutant provided evidence for the protonation of D75 upon full reduction of the protein and quinone.[22] This work is thus consistent with the presence of D75 at the quinone binding-site and suggests an important functional role for this residue. Clear information on specific interactions is, however, not available from any of these studies.

Stabilisation of the semiquinone radical in the Q_H site has been shown by various cw- and pulsed EPR studies of the Q_H semiquinone in the bacterial bo_3 QOX complex.[10,11,14–17] A multifrequency (9, 34, and 94 GHz) EPR study performed in QOX using bound quinones with ^{13}C-selectively labelled at either the 1- or 4-carbonyl carbon position revealed a significant difference between the A_{ZZ} components of hyperfine tensors of the two carbon atoms that provides some evidence for an appreciably asymmetrical spin density distribution attributed to a very asymmetric binding environment of the radical.[17] Grimaldi *et al.*[17] even postulated single-sided hydrogen bonding to the 1-oxygen position. ESEEM studies have

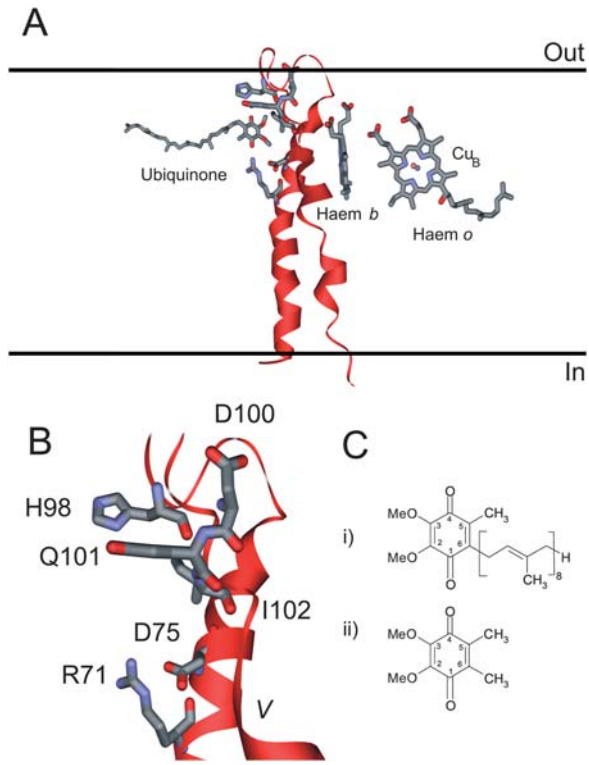

Fig. 1 The putative Q_H binding site in the cytochrome *bo*$_3$ ubiquinol oxidase (QOX) from *Escherichia coli* (*E. coli*). (A), Model of the quinone binding site in relation to the heme centres and an indicated membrane, according to Abramson *et al.*[19] (B), D75 is shown together with the residues suggested to participate in quinone/quinol binding and proton translocation. (C) Chemical structures of (i) the native ubiquinone-8 (UQ_8) and of (ii) 2,3-dimethoxy-5,6-dimethyl-1,4-benzoquinone (DDQ).

demonstrated that this semiquinone radical in QOX forms a hydrogen bond with a nitrogen atom either from the polypeptide backbone of the protein[16] or from an arginine side chain[17] and very recently studies of Lin *at al.* have identified N_ε of Arg71 as a H-bond donor.[23] Using a combination of 1D and 2D ESEEM and pulsed-ENDOR Yap *et al.*[24] have provided additional information about the exchangeable protons involved in hydrogen bonding to the semiquinone in the Q_H site of QOX. They observed three exchangeable protons with distinct hyperfine couplings (HFC's) in the immediate environment of the semiquinone radical.[24] After detailed analysis of the HFC's of both exchangeable and non-exchangeable (methyl) protons they proposed a neutral radical, rather than an anion radical form of the radical as the form of the semiquinone stabilised by the Q_H binding site. They supported their statement by subsequent studies of two mutants: D75E and D75H.[18]

Recently we have carried out a comprehensive systematic quantum-chemical study of various molecular models of ubisemiquinone radical anions using the complex situation in the Q_H binding site as the basis for our studies.[25] Comparison with experimental EPR and ENDOR results clearly supported an asymmetric hydrogen-bonding environment with two hydrogen bonds to the O_1 carbonyl oxygen and one hydrogen bond to the O_4 carbonyl oxygen, but a model with one more hydrogen bond on each side could not be excluded. All the models considered in our studies included an anionic semiquinone radical as the one being stabilised by a binding site.

In these studies it was shown that ^{13}C HFC's were most sensitive to asymmetrical changes in the spin density distribution in the semiquinone head group as a result of changes in the electrostatic environment around the semiquinone, whereas both the ^{1}H-HFC's (methyl) and g-tensor were shown to be less influenced.

The role of this asymmetry in electron and proton transfer is of great interest for understanding the principle behind proteins that convert two-electron donors for timely one by one sequential electron transfer on the basis of a radical mechanism. This has previously discussed in detail in bacterial reaction centres (*e.g.*[26]), where asymmetric binding of the quinone radical is suggested to be a prerequisite for efficient sequential electron transfer. In this work we use variants that perturb the hydrogen-bonding environment between the bound quinone and potential ligands and characterise them by the two-dimensional pulsed EPR techniques HYSCORE (HYperfine Sublevel CORElation) and DONUT-HYSCORE (DOuble NUclear coherence Transfer HYSCORE).

On the quantum-chemical side we extend our set of models to those having a neutral semiquinone radical as a stabilised cofactor in the Q_H site. In a simultaneous recent study Boesch *et al.*[27] also briefly addressed this problem. Here we provide a comprehensive discussion of various EPR parameters with the aim to establish the exact nature of the bound semiquinone.

Materials and methods

Sample preparation

The *E. coli* strain GO105/pJRHisA[28] was grown and isolated as described previously.[16] Wild-type bo_3 enzyme with bound UQ_8 was purified as described previously.[29] Native UQ_8 was removed by purification of QOX using *N*,*N*-dimethyldodecylamine *N*-oxide (LDAO) as the detergent, followed by detergent exchange with n-dodecyl-β-D-maltoside (β-DM). Reconstitution with exogenous 2,3-dimethoxy-5,6-dimethyl-1,4-benzoquinone (DDQ, see Fig. 1C, ii)) and UQ_2 analogues was performed directly in the EPR sample tube containing the protein, using quinone solutions dissolved in a very small amount of 2-propanol (1 μL). All samples were reduced with an excess of sodium ascorbate under a strict argon atmosphere and immediately frozen.

Site-directed mutagenesis of the pJRHisA plasmid,[28] transformed into GL101[30] has been reported previously.[22] Variant cytochrome bo_3 ubiquinol oxidase from *E. coli* containing one equivalent of bound UQ_8 was purified in n-dodecyl-β-D-maltoside according to the method described previously,[28] and concentrated to approximately 0.1 mM in 100 mM K-Phosphate buffer at pH 8. The presence or absence of ubiquinone was confirmed by FTIR spectroscopy as reported in[31] (data not shown).

The ubiquinone-10 ($UQ_{10}^{\cdot-}$) and 2,3-dimethoxy-5,6-dimethyl-1,4-benzoquinone ($DDQ^{\cdot-}$) anion radicals were generated by dissolving the respective quinone (approximately 1 mM) in slightly basic (potassium *tert*-butylate, 10-fold molar excess) anaerobic solutions of protonated 2-propanol. The solution was further deoxygenated in the EPR sample capillary by bubbling with purified oxygen-free argon for 2–3 min and then shock-frozen by immersion in liquid nitrogen. $UQ_{10}^{\cdot-}$ was also generated in the aprotic, apolar and glass forming ether 2-methyltetrahydrofuran (mTHF) under high vacuum conditions by potentiostatically controlled electrolysis using tetra-n-butylammonium perchlorate (TBAP) as supporting electrolyte using a electrochemical cell described in ref. 32.

EPR spectroscopy

X-band cw-EPR spectra were recorded on a Bruker eleXsys E500 spectrometer using a standard rectangular Bruker EPR cavity (ER4102T) equipped with an Oxford helium cryostat (ESR900). All measured g-values have been corrected for an offset

against a known standard (DPPH). X-band pulsed EPR measurements were performed on a Bruker eleXsys E-580 spectrometer using a standard dielectric resonator (MD5 W1) equipped with an Oxford helium (CF 935) cryostat. The microwave pulses were amplified using a 1 kW pulsed-TWT. In 3-pulse ESEEM spectroscopy[33] (Fig. 2B), the amplitude of the stimulated echo as a function of τ and T was measured at a frequency of approximately 9.6 GHz, at a magnetic field corresponding to the maximum intensity of the field swept spectrum where all orientations of the molecule with respect to the magnetic field contribute. The minimum pulse separation time T was 120 ns and was incremented in steps of 16 ns (800 data points); the duration of the $\pi/2$ pulse was 16 ns. Measurements were carried out at 20 K and τ values were varied from 120 to 440 ns in order to avoid suppression effects.[34]

Using hyperfine sublevel correlation spectroscopy (HYSCORE) the nuclear coherence within one electronic manifold is transferred by an additional MW pulse into the corresponding nuclear coherence within the other electronic manifold (Fig. 2C).[35] A 2D-FT leads to a 2D spectrum in frequency space with off-diagonal correlation peaks between hyperfine lines belonging to the same nucleus in both electronic manifolds. This is very helpful in unravelling complex hyperfine spectra with overlapping line contributions from different nuclei. 2D-HYSCORE spectra were recorded (Fig. 4c, e), where the echo amplitude is measured as a function of t_1 and t_2.[35] The durations of the $\pi/2$ and π pulses were optimised to 16 and 32 ns respectively, with equal amplitudes. A set of 512*512 data points was recorded. t_1 and t_2 were incremented in steps of 16 ns from their initial values. To remove the unwanted echoes, the appropriate 4-step phase-cycling procedures in the stimulated echo[36] and HYSCORE[37] experiments were applied.

The two-dimensional experiment double nuclear coherence transfer hyperfine sublevel correlation (DONUT-HYSCORE) is complementary to HYSCORE and is designed to obtain correlations between nuclear frequencies belonging to the

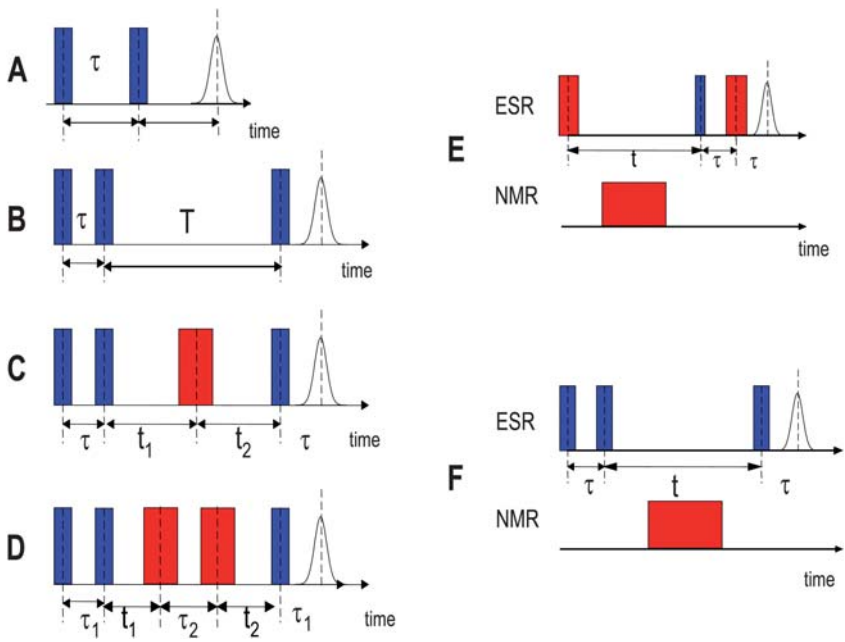

Fig. 2 EPR and ENDOR pulse sequences used in the experiments described in text where blue pulses denote $\pi/2$ pulses and red pulses denote π-pulses respectively. **(A)** Two-pulse (Hahn) echo,[103] **(B)** three-pulse (stimulated) echo,[33] **(C)** four-pulse echo (HYSCORE),[35] **(D)** five-pulse echo (DONUT-HYSCORE),[38] **(E)** Davies ENDOR,[64] **(F)** Mims ENDOR.[79]

same electron spin manifold and is particularly useful for ^{14}N nuclei (Fig. 4d & 4f). This is a five pulse sequence (Fig. 2D) whereby the echo amplitude is measured as a function of t_1 and t_2 whereby τ_1 and τ_2 are held constant.[38]

For 1D-stimulated echo ESEEM, prior to Fourier transformation, the time-domain echo decay was removed by subtraction using a polynomial function followed by zero filling to 1024 points and a tapering using a Hamming window. For 2D HYSCORE and DONUT-HYSCORE, prior to 2D Fourier transformation, the background decay in both t_1 and t_2 dimensions was subtracted using a polynomial function followed by zero-filling to 1024 points in both dimensions and tapering with a Hamming window. All 1D and 2D spectra are shown in the absolute value mode.

EPR theory

The Hamiltonian operator describing the magnetic interaction between an electron spin S = ½ (of the ubisemiquinone radical) and a nitrogen nucleus (nuclear spin $I = 1$) can be described in the high-field approximation by:

$$H = g_{eff}\beta_e B_0 S_Z - g_N\beta_N B_0 I_Z + \vec{S}\,\tilde{A}\,\vec{I} + \vec{I}\,\tilde{P}\,\vec{I} \quad (1)$$

where g_{eff} is the effective g-value and B_0, the external magnetic field, assumed to be directed along the z-direction. The second term in the Hamiltonian describes the Zeeman interaction of the nuclear spin I with B_0. The hyperfine coupling tensor $\tilde{A}$ consists of the isotropic contribution A_{iso} and the traceless tensor $\tilde{T}$ describing the anisotropic hyperfine coupling. The nuclear quadrupole interaction tensor, $\tilde{P}$ (with its principal values V_{XX}, V_{YY}, V_{ZZ}), is traceless by definition. In its principal axis system the final term in eqn (1) is expressed in the form

$$\vec{I}\,\tilde{P}\,\vec{I} = \kappa\left[3I_Z^2 - I^2 + \eta\left(I_X^2 - I_Y^2\right)\right] \quad (2)$$

where κ represents the quadrupolar coupling constant $e^2qQ/4h$, $\eta = |(V_{XX}–V_{YY})/V_{ZZ}|$ is the asymmetry parameter of the electric field gradient on the nucleus. e is the elementary charge, Q is the nuclear quadrupole moment and h is Planck's constant.

DFT computational details

Structure optimisation and models. In the absence of more specific structural information, the new, additional supermolecular models employed here consist of a neutral semiquinone molecule hydrogen-bonded by either N-methylformamide (nmf) or water, or both. Water molecules are not ideal H-bond donors because in more crowded models they create H-bonds to the oxygen of the methoxy substituent for which there is no experimental evidence. Here we have therefore selected a mixture of water and nmf molecules as H-bond donors.

As the nature of the isoprenoid side chain in case of a ubisemiquinone radical anion has been found both experimentally and computationally to only negligibly influence the g-tensor and most hyperfine parameters[39–41] it has been replaced by an ethyl group in our models (ubisemiquinone radical anion $UQ^{\cdot-}$; neutral ubisemiquinone radical $UQH^{\cdot}$). The resulting model complexes are shown later in Fig. 8.

All structures have been fully optimised at the density functional (DFT) level, using the gradient-corrected BP86 functional[42,43] and a DZVP Gaussian-type-orbital basis set.[44] SVP auxiliary basis sets[45] were used to fit the electron density (RI-DFT approximation). Unless stated otherwise, the calculations were performed with TURBOMOLE program (version 5.8).[46,47]

g-Tensor calculations. The g-tensor calculations employed the second-order perturbation approach delineated in ref. 48,49, which has been demonstrated to

provide unprecedented accuracy in calculations of g-tensors for organic radicals (see also a recent review on g-tensor calculations for organic radicals[50]). The Kohn–Sham orbitals were obtained with the TURBOMOLE program and involved the fitting of charge density but not of exchange–correlation potential. These calculations (at the RI-BP86/DZVP level) overestimate the most sensitive Δg_{XX} tensor of anionic semiquinone radicals systematically and require a scaling factor of 0.88 to provide agreement between supermolecular model calculations and experimental data in protic solution.[49,51] The same scaling has been applied to the neutral radicals. The unrestricted Kohn–Sham molecular orbital information from TURBOMOLE was transferred by appropriate interface routines to the MAG (magnetic resonance) property module of the in-house program ReSpect.[52] The one- and the two-electron spin–orbit (SO) operators were treated by the accurate and efficient all-electron atomic mean-field approximation (AMFI).[53,54] A common gauge origin for the external magnetic vector potential was chosen at the midpoint between the two carbonyl oxygen atoms. This is expected to be close to the centre of spin density. In our calculations, the g-tensor is defined as $\mathbf{g} = g_e(\mathbf{1}) + \Delta\mathbf{g}$, where $g_e = 2.002319$. We present and discuss g-shift components of (Δg_i) defined as corrections to the free electron value in ppm (that is, in units of 10^{-6}). Our approach includes not only the dominant second-order spin–orbit/orbital-Zeeman cross terms but also the relativistic mass correction (RMC) and the one-electron part of the spin–orbit gauge correction (GC) terms.[48,49]

Hyperfine tensor calculations. All hyperfine coupling parameters were computed in the usual nonrelativistic first-order approach, using the MAG-ReSpect[52] code based on unrestricted Kohn–Sham wave functions obtained with the TURBOMOLE[46,47] program. It is well-known that gradient-corrected functionals such as BP86 underestimate the spin polarisation in π-radicals and thus provide less accurate hyperfine couplings. In contrast to the optimisations and g-tensor calculations, the hyperfine calculations used therefore the B3LYP[55–57] hybrid functional (in nonlocal implementation, *cf.* ref. 58,59 for a discussion) in combination with the EPR-II[60] basis set (which is specifically designed for hyperfine calculations). Further test calculations with other functionals, and also with more extended EPR-III basis sets, provided only minor modifications.

EPR results and discussion

Both wild-type and variant QOX under reducing conditions give strong narrow EPR signals at $g \sim 2.0044$ using cw-EPR at 9.6GHz (data not shown, but see *e.g.*[16,21]). In all cases except D75H the observed EPR lineshape was partially resolved due to $^1H_{CH3}$ HFC's as has been observed and analysed previously.[17] In order to directly study the immediate environment of the semiquinone moiety in the Q_H binding site, 3-pulse ESEEM spectroscopy was performed at ~9.6 GHz (X-band). In order to avoid missing modulation frequencies due to suppression effects,[34] the echo decay was recorded at several τ values (data not shown). Fig. 3 displays the "suppression free" frequency-domain spectra, which are the skyline projections of the Fourier transform of the stimulated echo ESEEM spectra recorded at a series of different τ values. The spectra in Fig. 3 represent a series of QOX samples containing both the wild-type UQ8 (A) and 2,3-dimethoxy-5,6-dimethyl-1,4-benzoquinone (DDQ) substituted QOX (D) as well as variant QOX, D75E (B), D75H (C) and I102Q (E). The ESEEM data for QT QOX containing UQ_2 is very similar to that of the QOX containing the native quinone and has been published previously.[17]

In each spectrum at least four frequency components are clearly resolved: three intense narrow lines and another much broader line. In spectra A, B, D and E these narrow lines are at ~0.9, ~2.4 and ~3.3 MHz and the broad line has its maximum at ~5.2 MHz. Spectrum C from D75H has peaks at distinctly different frequencies.

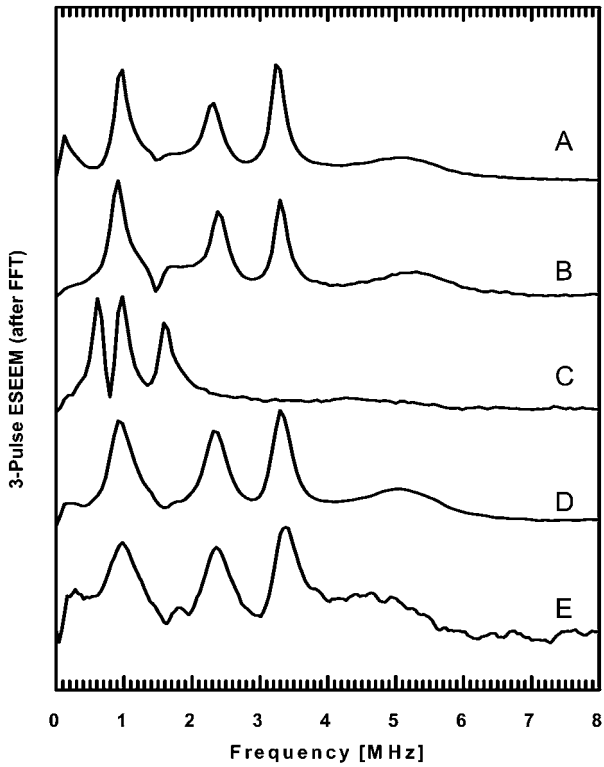

Fig. 3 X-band ESEEM spectra of QOX. Three pulse ^{14}N-ESEEM FT-spectra (absolute value mode) of the Q_H ubisemiquinone radical in the bo_3-type ubiquinol oxidase from *E. coli*. A) Wild-type, B) D75E, C) D75H, D) DDQ in QOX, E) I102Q. The echo envelope was recorded by varying the time between the second and third microwave pulses. Experimental conditions: $\pi/2$ pulse length: 12/16 ns, temperature: 20 K, microwave frequency: 9.764 GHz, shot repetition time: 50 ms. A background correction using a second-order polynomial function has been used to remove the decay of the echo amplitude due to relaxation processes. Spectra are the skyline projection of a series of three pulse ESEEM spectra recorded at 8–16 τ values varied from 120 ns in steps of 8/16 ns.

A characteristic proton matrix-peak appearing at about 14.8–15 MHz is also present in all the spectra (data not shown) but is not discussed in the following.

The simple additive relationship satisfied by three of the four peaks observed (*e.g.* the sum of the 0.9 MHz and 2.4 MHz frequencies equalling the 3.3 MHz frequency) and their typical profile allowed their assignment previously to ^{14}N ($I = 1$) nuclear transitions. This is a case where the so-called "cancellation condition"[61] is fulfilled, that is to say when the nuclear Zeeman and hyperfine interactions effectively cancel in one electron-spin manifold (*i.e.* $A/2 = \nu_I$)[16] (see Fig. 4A). In this manifold, the nuclear spin Hamiltonian reduces to the purely quadrupolar Hamiltonian and the ^{14}N nuclear quadrupolar resonance (NQR) transitions observed (the three, narrow low-frequency components) are given by the relationships

$$\nu_0 = 2\kappa\eta,\ \nu_- = \kappa(3 - \eta),\ \nu_+ = \kappa(3 + \eta) \tag{3}$$

where κ represents the quadrupolar coupling constant and η is the asymmetry parameter of the electric field gradient $\{q_{ii}\}$ on the nucleus. The cancellation condition of the effective field prevents any frequency dispersion related to the orientation of B_0, so that these lines reveal no anisotropic broadening, leading to this typical sharp profile. A moderate deviation from the exact cancellation would drastically

reduce the intensities of the observed peaks whereas their positions would remain almost constant.

The hyperfine manifold, where the nuclear-Zeeman and the hyperfine interactions are additive, gives rise to much broader resonances[61] and the only resolvable component is a double quantum transition line, $\Delta m_I = 2$, occurring at higher frequencies. This line has maximum intensity at a frequency, which is approximated by

$$\nu_{dq\pm} \approx 2[(\nu_I \pm A/2)^2 + \kappa^2(3 + \eta^2)]^{1/2} \quad (4)$$

where A is a secular component of the hyperfine coupling tensor determined mainly from its isotropic part in the case of a small anisotropic hyperfine tensor. A modest anisotropy of the hyperfine interaction affects mainly the line shape but not the frequency of this double quantum line.[61]

The application of eqn (3) to the three lines at 0.9, 2.4 and 3.3 MHz assigned, respectively, to ν_0, ν_- and ν_+ gives $\kappa = 0.94$ MHz, $\eta = 0.49$. From eqn (4), the assignment of $\nu_{dq\pm} = 5.2$ MHz leads to the value $A = 1.8 \pm 0.1$ MHz. Although this estimated A value deviates from the $2\nu_I$ value (*i.e.*, $|A_{iso} - 2\nu_I| = 0.34$ MHz), this deviation does not exceed $4K/3 \approx 1.25$ MHz, which is the limiting value for the validity of the cancellation condition. The so-called "intermediate K regime" for which the K value is close to the value of A/2, in case of a powder spectrum has been shown to be characterised by the absence of single quantum peaks and broadening of the double quantum peak.[61] These features are in accordance with our spectra.

The above theoretical analysis was strongly indicative for the interpretation of the data and it was further supported using HYSCORE experiments[16]; see later for a detailed discussion.

In the spectrum from D75H (Fig. 3c), again three/four frequency components are resolved: three narrow lines and possibly a weak broad line. These narrow lines are at ~0.61, ~0.97 and ~1.59 MHz and the broad line has its maximum at ~4.8 MHz.

Again, the simple additive relationship seems to be satisfied by the first three peaks (*e.g.* the sum of the 0.61 MHz and 0.97 MHz frequencies equalling the 1.59 MHz frequency) allowing their assignment to ^{14}N ($I = 1$) nuclear transitions in the "cancellation condition" case.[61] Using eqn (3), κ (the quadrupolar coupling constant) and η (the asymmetry parameter of the electric field gradient $\{q_{ii}\}$ on the nucleus) could be determined. The only resolvable component from the other spin manifold is the double quantum transition line, $\Delta m_I = 2$, which is observed at ~4.8 MHz. Using eqn (4), this leads to a value of $A = 2.3 \pm 0.1$ MHz.

This analysis provides a possible interpretation of the data. However, in order to confirm all of these assignments HYSCORE spectroscopy has been employed to demonstrate the correlations between these frequencies which worked well for the wild-type UQ_8 containing QOX[16]. Due to the predicted binding site model (Fig. 1A) it is important to demonstrate that there is only a single strongly interacting nitrogen nucleus and such 2D correlation spectroscopy can be used to eliminated or resolve potential spectral overlap. A further exacting control of whether only a single nitrogen nucleus is involved can be performed using DONUT-HYSCORE spectroscopy, and, indeed, this can also confirm that the observed peaks originate from only one nitrogen nucleus as the expected HYSCORE correlation peaks are rather weak and difficult to observe (Fig. 4c and 4e).

In HYSCORE experiments (Fig. 4c) cross peaks between hyperfine frequencies belonging to different M_s manifolds of the same nucleus[35] are observed, see Fig. 4b for a descriptive cartoon. Therefore, the peaks at (ν_{dq},ν_0), (ν_{dq},ν_-) and (ν_{dq},ν_+) are expected. The HYSCORE spectrum of Q_H^- from wild-type and D75H are presented as contour plots in Fig. 4c and 4e. The on-diagonal features in both quadrants have a dominant intensity and are due to a weak inversion of the π pulse.[37] The off-diagonal features are quite symmetrical with respect to the diagonals in both quadrants, which agrees well with theory.[62] While for the wild-type sample intense cross peaks at (5.2, 3.3 (ν_+)) and two weaker cross peaks at (5.2, 2.4 (ν_-)) and

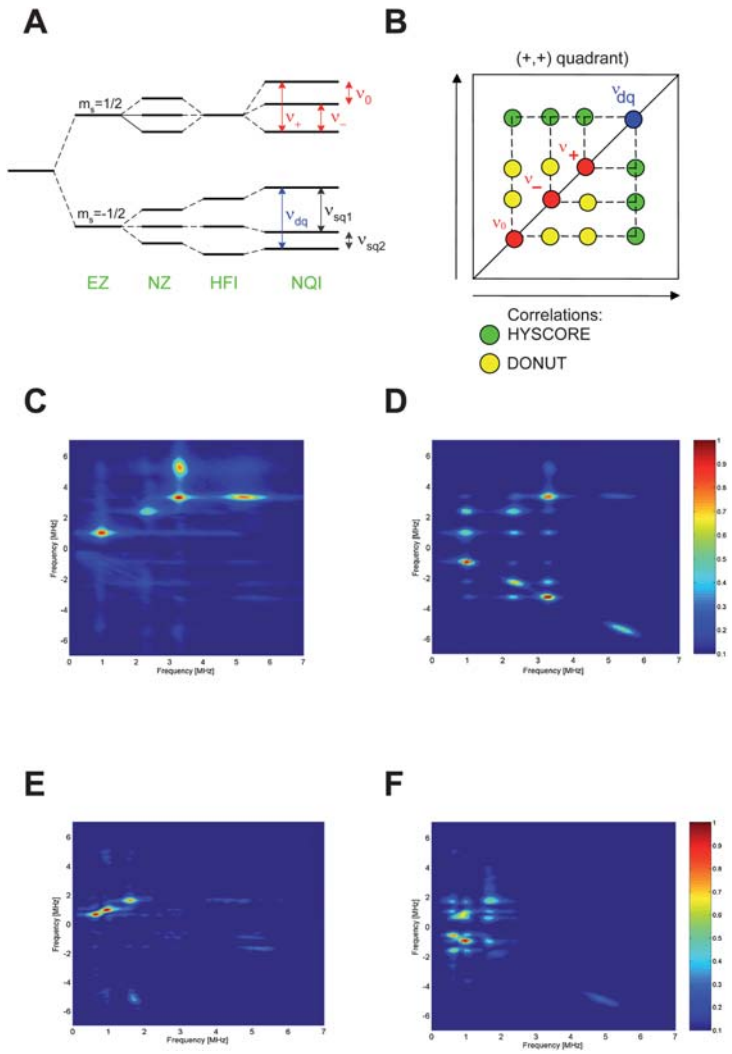

Fig. 4 X-band HYSCORE and DONUT-HYSCORE spectra of QOX. (A) This is a simplified diagram to display the energy level splitting in an external magnetic field of an unpaired electron (S = ½) interacting with one ^{14}N ($I = 1$) nucleus in the region of exact cancellation.[61] EZ is the electron-Zeeman splitting; NZ is the nuclear Zeeman splitting; HFI is the hyperfine splitting for one ^{14}N nucleus with $A_{iso} \cong 2\nu_I$; NQI is the nuclear quadrupolar interaction. The 6 possible nuclear transition frequencies from the three nuclear energy sublevels in each of the two electron spin manifolds ($m_s = \pm$ ½) are indicated. In the case of exact cancellation three sharp transitions (ν_+, ν_- and ν_0 labelled in red) are observable from one manifold, whereas only the ν_{dq} (labelled in blue) is observed from the other manifold. (B) HYSCORE and DONUT-HYSCORE are four and five pulse two dimensional correlation techniques which observed the correlation of frequencies from different (HYSCORE) and within the same (DONUT-HYSCORE) electron spin manifolds. This scheme indicates the correlations which can be observed using HYSCORE (in green) and DONUT-HYSCORE (in yellow) in the case of exact cancellation. (C) and (E) ^{14}N-HYSCORE spectrum (absolute value mode) of $Q_H^{\cdot}$ in wt-QOX (C) and $Q_H^{\cdot}$ in D75H-QOX (E). In this experiment the time between the first two (both $\pi/2$) microwave pulses was $\tau = 132$ ns and the times t_1 (between the second ($\pi/2$) and third (π) microwave pulses) and t_2 (between the third (π) and fourth ($\pi/2$) microwave pulses) were incremented in steps of 16 ns from their initial values and 512 points were recorded in each dimension. Experimental conditions: $\pi/2$ and π pulse lengths: 8 ns and 16 ns respectively, temperature: 20 K, microwave frequency: 9.764 GHz, shot repetition time: 50 ms. (D) and

(5.2, 0.9 (ν_0)) MHz are clearly observed, cross peaks in the D75H spectrum are much more difficult to observe (Fig. 4e). In the wild-type spectrum the appearance of these cross peaks provides an unambiguous assignment of the 5.2 MHz peak to ν_{dq} and not to a nuclear transition frequency of a second nitrogen nucleus and is a first control for the wild-type. Such cross peaks are far less obvious in the D75H variant (Fig. 4e)

In order to confirm our assignments in the D75H variant DONUT-HYSCORE is used.[38] DONUT-HYSCORE (Fig. 2D) is a five-pulse variant of the HYSCORE experiment where the spectra exhibit only cross-peaks between hyperfine frequencies belonging to same M_s manifolds of the same nucleus.[38] Therefore only peaks at (ν_+,ν_0), (ν_+,ν_-) and (ν_0,ν_-) are expected (see Fig. 4b for a descriptive cartoon). The DONUT HYSCORE spectra of $Q_H^{\cdot}$ for both wild-type and D75H are presented as contour plots in Fig. 4d and 4f. This is the first time that DONUT-HYSCORE spectra of a protein-bound semiquinone species have been reported. The on-diagonal features in both quadrants have a dominant intensity again due to a weak inversion of the π pulse.[37] The use of matched microwave pulses[63] permits the removal of these on-diagonal features using, in this case, pulses of 72 ns, but do not change the interpretation at all (data not shown).

The off-diagonal features are quite symmetrical with respect to the diagonals in both quadrants, and this agrees well with the theory.[62] While for the wild-type sample the cross peaks at (3.3, 2.4 (ν_+)), (3.3, 0.9 (ν_-)) and (2.4, 0.9 (ν_0)) MHz are clearly observed, cross peaks are also now clearly resolved at (1.6, 0.9 (ν_+)), (1.6, 0.6 (ν_-)) and (0.9, 0.6 (ν_0)) for the D75H variant, supporting the previous assignment to a single nitrogen nucleus.

In Fig. 5 we show the pulsed ENDOR spectra of QOX using the Davies pulse ENDOR sequence[64] (Fig. 2E) which does not suffer from "blind spots" across the spectrum and is suitable for resolving large ^{1}H-hyperfine couplings. The native semiquinone UQ_8 in QOX is measured at pH 6 (Fig. 5A) and pH 8 (Fig. 5B), where broad couplings indicated by the two vertical lines are assigned to the $A_{\|}$ component of the nearly axial methyl HFC tensor (position 5 in Fig. 1C). Interestingly there is a clear and significant pH dependency of this HFC (Fig. 5A and 5B). The axial tensor of this CH_3 coupling is more clearly resolved when the sample is H_2O/D_2O exchanged (Fig. 5C). This HFC has been characterised in detail previously using both ENDOR and EPR spectral analyses *e.g.*,[14,15,17] and reflects the unpaired electron-spin density at the attached (ring) carbon atom *via* the McConnell relationship.[41,65] This provides a first probe of the electron density distribution in the semiquinone head group, see *e.g.* ref. 26,41 for a discussion of the electron density distribution in anionic semiquinones. Here we will only use the position of this resonance as a marker when comparing QOX containing different quinones and also in variants. As has been shown previously,[17] substituting UQ_8 for UQ_2, which has a much shorter isoprenyl chain, does not significantly alter the spin density distribution in the semiquinone head group (Fig. 5D), although there had been discussion of the importance of this side chain in the tight binding at this site as compared to the Q_L site.[66] It appears that it is the protein binding pocket itself which determines the asymmetric spin density distribution on the semiquinone rather than the fact that the molecule itself is asymmetric. This is evidenced (Fig. 5E) by the use of the symmetric molecule 2,3-dimethoxy-5,6-dimethyl-1,4-benzoquinone (DDQ, see Fig. 1C, ii). Spectral simulation (dotted line) clearly reveals two distinct methyl HFC's with

(F) ^{14}N-DONUT-HYSCORE spectrum (absolute value mode) of $Q_H^{\cdot}$ in wt-QOX (D) and $Q_H^{\cdot}$ in D75H-QOX (F). Again in this experiment the time between the first two microwave pulses was $\tau = 132$ ns and the times t_1 (between the second and third microwave pulses) and t_2 (between the fourth and fifth microwave pulses) were incremented in steps of 16 ns from their initial values and 512 points were recorded in each dimension. The time between the third and fourth pulses (both π pulses) was held constant (200 ns). Experimental conditions: $\pi/2$ and π pulse lengths: 8 ns and 16 ns respectively, temperature: 20 K, microwave frequency: 9.764 GHz, shot repetition time: 50 ms

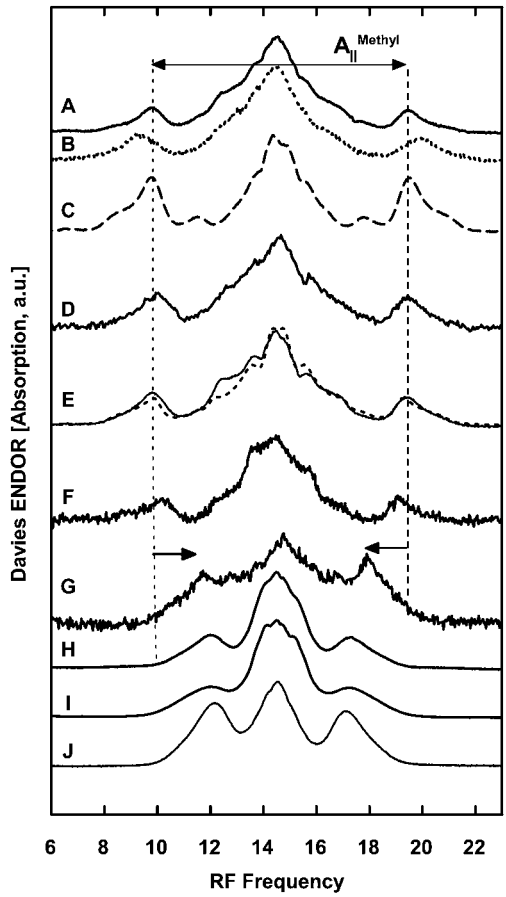

Fig. 5 Davies ^{1}H-ENDOR[64] spectra of the *bo*$_3$-QOX of *E. coli* (A–G) under reducing conditions and model semiquinone radicals in organic solvents (H–J). (A) native UQ_8 at pH6; (B) native UQ_8 at pH8; (C) native UQ_8 after H_2O/D_2O buffer exchange; (D) after reconstitution with UQ_2; (E) after reconstitution with DDQ (dotted line; simulation); (F) native UQ_8 in D75E; (G) native UQ_8 in D75H; (H) $UQ_{10}^{\cdot-}$ in slightly basic 2-propanol; (I) $UQ_{10}^{\cdot-}$ generated electrochemically in dimethoxyethane [32]; (J) $DDQ^{\cdot-}$ in slightly basic 2-propanol. Experimental conditions: Davies ^{1}H-ENDOR; microwave π–pulse length = 200 ns; radio frequency π–pulse length = 9 μs; and T = 20 K. The two dotted vertical lines indicated the splitting arising from the $A_{\|}$ component of the methyl (CH_3) hyperfine tensor.

the following values; A_{CH3}[1]: $A_{\|}$ = 12.5 MHz, $A_{\perp}$ = 8.4 MHz and A_{CH_3}[2]: $A_{\|}$ = 4.9 MHz, $A_{\perp}$ = 2.0 MHz (Fig. 5E and Table 5) as compared to the typical values for UQ_8 in QOX of A_{CH_3}: $A_{\|}$ = 12.8 MHz, $A_{\perp}$ = 8.0 MHz (Fig. 5A and Table 5) and of $DDQ^{\cdot-}$ in frozen 2-propanol of $A_{\|}$ = 8.0 MHz, $A_{\perp}$ = 5.3 MHz (Fig. 5J and Table 5) and $UQ_{10}^{\cdot-}$ in frozen 2-propanol of $A_{\|}$ = 8.5 MHz, $A_{\perp}$ = 4.8 MHz (Fig. 5H and Table 5). For comparison's sake, Davies ENDOR of $UQ_{10}^{\cdot-}$ in frozen aprotic mTHF is also shown where no H-bonds are formed (Fig. 5I and Table 5). The spin density distribution of DDQ in QOX is asymmetric but has clearly not reached the limit of a mono-protonated neutral semiquinone state where a more dramatic alteration of such hyperfine couplings would be expected as has been shown previously using DFT calculations.[25,67] Using CIDEP spectroscopy, the limiting case of a monoprotonated benzosemiquinone has indeed been studied, where such couplings can increase by a factor of 2 as compared to the anionic

semiquinone form.[68] In the variant D75E the methyl HFC is not altered significantly (Fig. 5F), whereas, in D75H, it is reduced significantly (see arrows in Fig. 5G).

The Q_H site is known to bind quinone much more tightly than the Q_L site whose quinone may exchange with the ubiquinol pool.[66] Unlike the Q_o and Q_i sites of the cytochrome bc_1 complex, and the Q_B site of the photosynthetic RC, the Q_H site appears not to be in dynamic equilibrium with this membrane quinone pool. The conditions that have been used for our study served to remove weakly bound ubiquinone but to leave the strongly bound ubiquinone at this high-affinity centre.

ESEEM spectroscopy carried out on the stabilised $Q_H^{\cdot}$ radical exhibited strong ESEEM modulations and using two-dimensional HYSCORE spectroscopy, this signal has been previously assigned to one nitrogen nucleus with quadrupolar parameters $\kappa = 0.94$ MHz and $\eta = 0.49$ directly interacting with the ubiquinone radical where the case of "cancellation condition" is fulfilled.[16]

Although it was not possible to identify the origin of the nitrogen signal solely by means of the ESEEM data, useful indications were obtained by comparison of the ^{14}N nuclear quadrupolar parameters (κ, η) determined from the ESEEM data, with nuclear quadrupole resonance (NQR) data available from the literature (see Fig. 6). The values for κ and η found in this earlier work were found to be similar to those found in NQR studies of the peptide nitrogens in small di- and tripeptides[69,70] and to the reported cases of ESEEM data arising from the modulation of an amide nitrogen of the peptide backbone in respiratory and in photosynthetic protein complexes.[71–73] It was noted at that time that no histidine nitrogen, whose quadrupolar parameters have been well characterised in other quinone binding sites (*e.g.* in $Q_A^{\cdot -}$ in bRCs) using ESEEM spectroscopy,[71,72,74] was detected in the Q_H binding site. Previously this had been predicted based on a classification study of known quinone binding sites[75] and from molecular modelling in the X-ray crystal structure (see Fig. 1B and the discussion in ref. 19).

There are, however, very early studies of NQR data on nitrogen containing compounds whose chemical structure is similar to that of an arginine side-chain[76] giving ^{14}N nuclear quadrupolar parameters (κ, η) similar to those observed in WT-QOX. The validity of such NQR parameters has been further substantiated

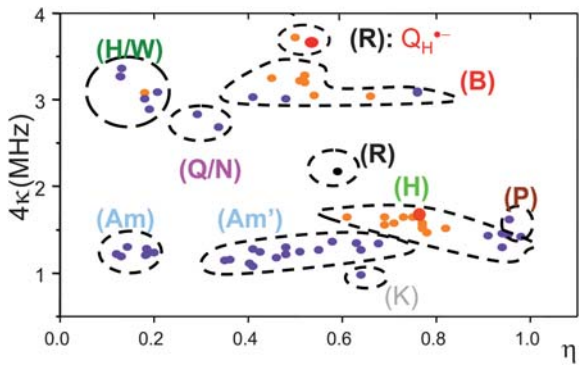

Fig. 6 Two-dimensional plot of quadrupolar parameters of ^{14}N interactions of protein bound semiquinones as measured by ESEEM spectroscopy (orange) and ^{14}N NQR of amino acids and peptides (purple). The values of (4κ,η) obtained for wt-QOX (arginine N(ε)) and D75H-QOX (histidine N(δ)) are indicated as red circles. See ref. 69 and references therein for ^{14}N-NQR data. (H/W) Indole, tryptophan, and histidine N(ε) nitrogen,[82,104]; (Q/N) glutamine and asparagine NH_2 nitrogen; (B) backbone nitrogen, peptide, di- and tripeptide, triglycine, [71,72,74]; (Am) and (Am′) NH_3^+ amino group nitrogen, (K) NH_3^+ lysine nitrogen, (P) proline nitrogen, (H) and histidine N(δ) nitrogen.[71,72,74,80,105] (R) arginine N(ε).[16,23] Recently First ^{14}N NQR quantum chemical calculations (DFT) have also been performed on quinone-histidine model compounds and in proteins.[73,106]

using ESEEM techniques on spin-labelled compounds containing NH_2 substituents (see page 94 in ref. 77), suggesting that the interaction observed in WT QOX may arise from Arg71.

The large isotropic hyperfine coupling value between $Q_H^{\cdot}$ and ^{14}N ($A_{iso} \approx 1.8$ MHz) demonstrates a delocalisation of the electron spin density of $Q_H^{\cdot}$ onto the nitrogen. This is much larger than a purely dipolar coupling estimated over a distance of 3–3.5 Å (<0.2 MHz) suggesting that spin density is directly transferred from the quinone radical to the amino acid nitrogen and would indicate the presence of a hydrogen bond between one of the carbonyl oxygens of $Q_H^{\cdot}$ and the nitrogen nucleus.

Use of ^{15}N labelling together with both HYSCORE and ENDOR spectroscopy allows us to a) unequivocally assign these observed frequencies to ^{14}N nuclei (Fig. 7a) and b) to accurately determine the distance between the interacting nitrogen nucleus and the carbonyl oxygen atom of the quinone moiety in the case of the matching condition (*i.e.* $A_{iso} = 2\nu_n$).[78] Two transitions ν_α and ν_β are observed in the ^{15}N-HYSCORE spectrum (Fig. 7b). One of them is also seen in the Mims ENDOR[79] spectrum (Fig. 7c) and the ν_α transition is approximately equal to $3|T|/4$ and $\nu_\beta \sim 2\nu_n$. This allows a determination of T whereby $T = g_n g_e \beta_n \beta_e / h^3$ (with the fundamental constants having their usual meaning). Hence it is possible to use these observed frequencies to determine this distance (r) using a simple point-dipole model. Assuming a typical oxygen spin density of 0.2 for *para*-benzosemiquinones[41] this gives an O–N distance of 2.25 Å. Care however needs to be taken (see ref. 80 for an example where this was not considered) as this is clearly an underestimation due to the rest (0.8) of the partial spin density spread over the rest of the quinone head group moiety and indeed by taking all of this spin density distribution into consideration this results in an O–N distance of 2.5–2.6 Å which indicates an H-bond length of 1.5–1.6 Å.

Experiments performed with ^{13}C-labelled quinones have also clearly demonstrated a strong asymmetry in the spin-density distribution within the semiquinone and that the observed interaction with a nitrogen nucleus must occur *via* the carbonyl oxygen at position 1 *i.e.* adjacent to the isoprenyl side-chain.[17] This asymmetry has also been inferred from ENDOR experiments[14] although this had previously been disputed by earlier cw-ENDOR experiments performed by other groups.[15]

ESEEM experiments performed on the variants D75E, which is fully active and I102Q, which shows a slightly reduced activity, do not indicate significant alteration of this interaction (Table 1), and indeed the other observed spectroscopic parameters, *e.g.* the ^1H-ENDOR spectrum, are also unaltered (Fig. 5) suggesting that the spin-density distribution in this species is unchanged. In the variant D75H, however, which shows no activity, a completely different interacting nitrogen nucleus is observed. Its assignment, based on the quadrupolar coupling parameters, is clearly to a histidine residue (see Table 1). The rearrangement of the spin-density distribution and specifically the methyl hyperfine coupling which is no longer resolved in the EPR spectrum and which is still clearly observed in the ^1H-ENDOR spectrum (Fig. 5) suggest that this histidine residue is indeed His98 and not the residue introduced by the mutagenesis. For a detailed discussion of the shifts in spin density distribution in anionic semiquinones see *e.g.* ref. 26,41.

Quantum-chemical results and discussion

(i) Structures of model complexes

Fig. 8 shows the optimised structures for all of the chosen new neutral semiquinone model systems of (i) the naked neutral semiquinone radical ($UQH^{\cdot}$) with a hydrogen atom covalently bound to either the O_1 or the O_4 carbonyl oxygen, (ii) $UQH^{\cdot}$ with single-sided hydrogen bonding to O_1 and O_4, respectively, (iii) $UQH^{\cdot}$ with symmetric or asymmetric double-sided hydrogen bonding. Out-of-plane angles γ of hydrogen

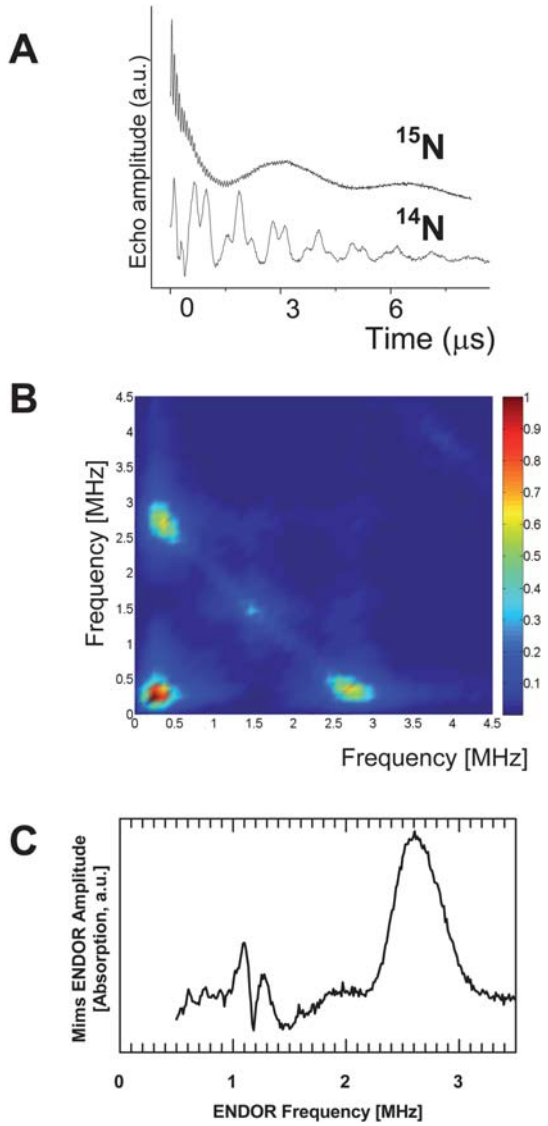

Fig. 7 ESEEM, HYSCORE and ENDOR of ^{15}N labelled QOX. (A) Time-domain three-pulse ESEEM spectra of $Q_H^{\cdot}$ in ^{14}N and ^{15}N globally labelled QOX recorded at 20 K. Experimental conditions: $\pi/2$ pulse length, 16 ns; microwave frequency, 9.64 GHz; shot repetition time, 50 ms. (B) HYSCORE spectrum (absolute value mode) of $Q_H^{\cdot}$ in ^{15}N-labelled QOX. In this experiment the time between the first two (both $\pi/2$) microwave pulses was $\tau = 128$ ns and the times t_1 (between the second ($\pi/2$) and third (π) microwave pulses) and t_2 (between the third (π) and fourth ($\pi/2$) microwave pulses) were incremented in steps of 32 ns from their initial values and 256 points were recorded in each dimension. Experimental conditions: $\pi/2$ and π pulse lengths: 16 ns and 12 ns (optimised for maximal echo inversion) respectively, temperature: 20 K, microwave frequency: 9.764 GHz, shot repetition time: 20 ms. (C) Mims ^{1}H-ENDOR[79] spectra of $Q_H^{\cdot}$ in ^{15}N-labelled QOX under reducing conditions. Experimental conditions: $\tau = 132$ ns, microwave π–pulse length = 48 ns; radio frequency π–pulse length = 28 μs; shot repetition time, 20 ms and $T = 20$ K.

bonds vary from 0° up to 90° (Table 2; *cf.* definition of γ in Fig. 8b). Unlike our previous studies on models involving semiquinone radical anion,[25] where dihedral angles γ were typically below 30°–40°, significantly different conformations of

Table 1 Nuclear quadrupolar parameters of ^{14}N nuclei interacting with protein-bound semiquinones and of ^{14}N in amino acids

Species	e^2qQ/h (MHz)	η	Reference
Rb. sphaeroides ($Q_A^{\cdot-}$)	1.65 3.05	0.73 0.54	*e.g.* 71
Rb. sphaeroides ($Q_B^{\cdot-}$)	1.65	0.61	*e.g.* 71
Photosystem II ($Q_A^{\cdot-}$)	3.25 1.60	0.45 0.70	*e.g.* 72
Quinol Oxidase ($Q_H^{\cdot-}$) wild-type	3.76	0.49	16
$UQ_2^{\cdot-}$	3.75	0.50	This work
$DDQ^{\cdot-}$	3.76	0.50	This work
D75E	3.72	0.50	This work
D75H	1.70	0.72	This work
Q101L	3.68	0.50	This work
Imidazole-semiquinone complex – DFT	1.5–1.9	0.6–0.7	73
Histidine	1.44 (N_δ-H) 3.36 ($N\varepsilon$)	0.91 0.13	89 89
Triglycine	3.01	0.48	70

methoxy substituents were found for the neutral as compared to the anionic semiquinone radical. For the neutral radical (hydroxyl group at C_1 side) values of θ_1 vary between 81° and 151°, and those of θ_2 vary between 6 to –65° (for the neutral radical with the hydroxyl group at the C_4 side the values are respectively similar). The methoxy group distal to the hydroxyl group if possible creates a weak H-bond to the neighbouring carbonyl oxygen, which is easily replaced by the provided water molecule. For an anionic semiquinone radical in the majority of cases both methoxy substituents were on the same side of the ring with θ_1 near 130°–140° and θ_2 near −55° to −60°.

Strong hydrogen bonding to O_1 was suggested by a number of previous studies.[81] Moreover, recent studies of Yap *et al.*[18,24] actually insisted on a hydrogen atom being covalently bound to O_1. Hence our study here focuses on the models with the hydroxyl oxygen bound to C_1. However, models with the hydroxyl oxygen bound to C_4 are considered for completeness. For some of the models more than one minimum structure was found. These varied in energy by up to 35 kJ mol^{-1} but gave similar EPR parameters (see below).

The computed length of a hydrogen bond to a hydroxyl oxygen strongly depends on the conformation of the covalently bound hydrogen. Long hydrogen bonds are computed for models with the hydroxyl hydrogen oriented in the plane of the semiquinone radical even for the models with only one hydrogen bond. Large out-of-plane angles of the hydroxyl hydrogen (*e.g.* 2/0-b 1HO–1HO) enforce hydrogen bonds even shorter than those found for semiquinone radical anion models.[25] A second water molecule, introduced as a potential hydrogen-bond donor on either O_1 or O_4 sides, always imposed a strong out-of-plane conformation on one of them with a simultaneous relocation of a second one to bridge between the first water molecule and a methoxy oxygen. This effect is due to the steric hindrance of the substituents of ubisemiquinone. Here it should be mentioned however that

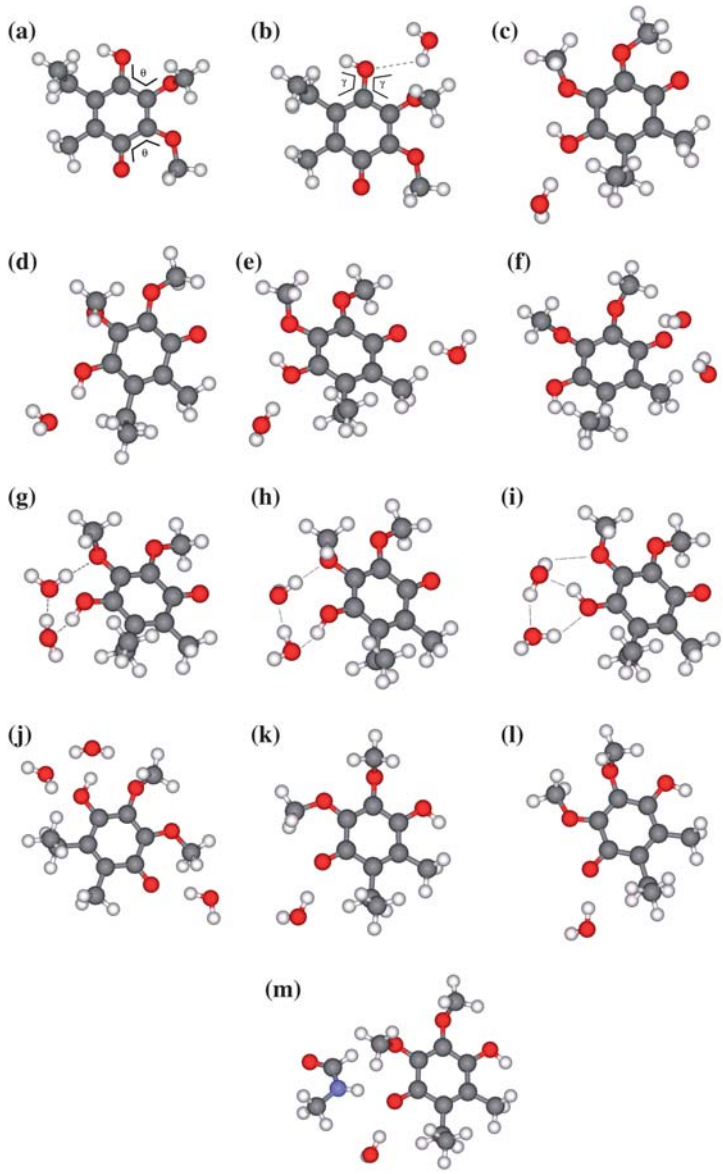

Fig. 8 Optimised structures of supermolecular model complexes. Numbers n/m indicate the number of hydrogen bonds to O_1 and O_4, respectively, and the labels HO and HN indicate a water molecule and an N-methylformamide molecule, respectively. *Models for neutral ubisemiquinone radical with hydroxyl group at O_1 position* (a–j): (a) 0/0 model; definition of methoxy dihedral angles θ_1 and θ_2; (b) 1/0-a model 1HO; definition of hydrogen-bonding dihedral angle γ; (c) 1/0-b model 1HO; (d) 1/0-c model 1HO; (e) 1/1 model 1HO–4HO; (f) 0/2 model 4HO–4HO; (g) 2/0-a model 1HO–1HO; (h) 2/0-b model 1HO–1HO; (i) 2/0–c model 1HO–1HO; (j) 2/1 model 1HO–1HO–4HO. *Models for neutral ubisemiquinone radical with hydroxyl group at O_4 position* (k–m): (k) 1/0-a model 1HO; (l) 1/0-b model 1HO; (m) 2/0 model 1HO–1HN.

experimental evidence from $Q_H^{\cdot}$ in QOX do not suggest hydrogen bonding to the methoxy substituents.[31] In some of the models one of the water molecules turned out not to be a donor but an acceptor of a hydrogen bond from the hydroxyl group. It was shown previously for semiquinone radical anions that hydrogen bond

Table 2 Hydrogen bond lengths, hydrogen-bond dihedral angles,[a] and methoxy-group out-of-plane dihedral angles[a]

Model	d (H···O) in Å; absolute dihedral angle γ in deg						Dihedral angles θ of methoxy groups	
	O_1/O_4–H;	γ O_1···HO;	γ O_1···OH;	γ O_4···HO;	γ O_4···HO;	γ	θ_1;	θ_2
Models for neutral ubisemiquinone radical with hydroxyl group at O_1 position								
0/0	0.98;	−3					105;	15
1/0-a 1HO	0.98;	−5	2.93;	17			110;	16
1/0-b 1HO	0.99;	1	2.01;	1			121;	6
1/0-c 1HO	0.99;	−8	1.90;	−16			105;	22
1/1 1HO-4HO	0.99;	1	2.02;	1	1.85;	13	121;	16
0/2-a 4HO-4HO	0.98;	−2			2.15;	46	1.91; −42	81; −57
0/2-b 4HO-4HO	0.99;	1			2.16;	45	1.89; −40	142; −61
1/2-a 1HO-4HO-4HO	1.00;	−9			2.21;	56	1.89; −36	151; −65
1/2-b 1HO-4HO-4HO	0.99;	0	2.06;	−14	2.20;	50	1.89; −35	144; −62
1/2-c 1HO-4HO-4HO	0.98;	0	2.32;	−6	2.18;	49	1.91; −42	146, −63
2/0-a 1HO-1HO	1.02;	−65	1.64;	−94			86;	13
2/0-b 1HO-1HO	1.02;	−60	1.64;	−91			91;	9
2/0-c 1HO-1HO	1.02;	4	2.05;	−72	1.70;	15	112;	17
2/1 1HO-1HO-4HO	1.02;	4	2.07;	−85	1.68;	16	1.83; 60	112; 8
Models for neutral ubisemiquinone radical with hydroxyl group at O_4 position								
0/0	0.99;	−177					119;	16
1/0-a 1HO	0.98;	1	1.88;	1			−9;	−105
1/0-b 1HO	0.98;	1	1.87;	−3.7			−164;	−75
2/0 1HO-1HN	0.98;	1.14	1.90;	14	2.05;	32	62;	−76

[a] Cf. Fig. 8a,b for a definition of the dihedral angles.

preferences are strongly coupled to the conformation of the methoxy substituents. As expected, the same relation is found for a neutral semiquinone radical except that here methoxy substituents adopt a larger range of dihedral angles θ (Table 2, see definition of θ in Fig. 8a). Nearly in-plane conformations are found for the methoxy group distal to the hydroxyl oxygen except for the models where a water molecule bridges between carbonyl and methoxy oxygen. Simultaneously, values between 81°–151° were computed for the dihedral angle of the proximal methoxy group. Optimisations carried out from different starting points all resulted in similar conformations.

(ii) g-Tensors

Table 3 compares computed g-shift tensors with experimental data in a variety of environments as well as with published data[25] computed for our best models of the semiquinone radical anion in the Q_H site. The experimental value of Δg_{XX} for the Q_H site is notably lower than data for the Q_A and Q_B sites of bacterial photosynthetic reaction centres or even for isotropic 2-propanol solution. As these reference systems feature extensive (double-sided) hydrogen bonding and a low Δg_{XX} is representative of strong hydrogen bonding, we must conclude that the low Δg_{XX} can only be explained by strong hydrogen bonding.[25]

Table 3 g-Shift tensors (ppm) for semiquinone radical models

Model[a]	Δg_{XX}[b]	Δg_{YY}	Δg_{ZZ}
Models for neutral ubisemiquinone radical with hydroxyl group at O_1 position			
0/0	5306 (4669)	3115	−29
1/0-a 1HO	5360 (4717)	3118	−30
1/0-b 1HO	5396 (4748)	3113	−36
1/0-c 1HO	5206 (4580)	3075	−33
1/1 1HO-4HO	4557 (4010)	2937	−31
0/2-a 4HO-4HO	3963 (3487)	2974	−137
0/2-b 4HO-4HO	3809 (3351)	3009	−128
0/1-a 1HO-4HO-4HO	3924 (3453)	2867	−103
0/1-b 1HO-4HO-4HO	3912 (3442)	3010	−114
0/1-c 1HO-4HO-4HO	3988 (3509)	2903	−129
2/0-a 1HO-1HO	5617 (4943)	3064	16
2/0-b 1HO-1HO	5577 (4907)	3035	13
2/0-c 1HO-1HO	5342 (4700)	3103	−33
2/1 1HO-1HO-4HO	4878 (4293)	2998	176
Models for neutral ubisemiquinone radical with hydroxyl group at O_4 position			
0/0	5262 (4630)	3133	−32
1/0-a 1HO	4706 (4330)	2985	−82
1/0-b 1HO	4622 (4252)	3024	−52
2/0 1HO-1HN	4016 (3695)	2950	85
Models for ubisemiquinone radical anion from ref. 25			
2/1-a 1HO-1HN-4HO	4660 (4101)	3031	−105
2/1-b 1HO-1HN-4HO	4766 (4194)	3019	−92
2/1-c 1HO-1HN-4HO	4804 (4228)	3018	−84
2/1-d 1HO-1HN-4HO	4786 (4212)	3020	−58
Experimental data			
$Q_H^{\cdot-}$ *in bo*$_3$*-QOX*[c]	*3611*	*3111*	*−119*
$Q_A^{\cdot-}$ in Zn-bRCs[d]	4300	3100	−100
$Q_A^{\cdot-}$ in Zn-bRCs[e]	4170	3000	−220
$Q_B^{\cdot-}$ in Zn-bRCs[e]	3940	2950	−220
UQ-10$^{\cdot-}$ in *i*PrOH[f]	4140	3100	−100
UQ-3$^{\cdot-}$ in *i*PrOH[g]	3900	2940	−220
UQ-3$^{\cdot-}$ in DME/MTHF[g]	4680	3050	−300
A_1^- in PS–I [h]	3900	2750	−140
A_1^- in PS–I [i]	3930	2710	−49

[a] *cf.* Fig. 8. [b] Values scaled by 0.88 in parentheses. [c] W-band EPR in *bo*$_3$-QOX.[17] [d] W-band EPR for zinc-substituted bRC.[39] [e] Q-band EPR in zinc substituted bRC of *Rhodobacter* (*Rb.*) *sphaeroides* R-26, with fully deuterated UQ-10$^{\cdot-}$.[90] [f] W-band EPR in frozen 2-propanol.[39,90] [g] Q-band EPR in 2-propanol-d_8 or DME/MTHF mixtures, respectively.[91] [h] Transient spin-polarised W-band EPR on $P_{700}^{\cdot+}A_1^-$ in a PS–I single crystal.[92] [i] Photoaccumulated A_1^- at 283 GHz.[93]

Similar to our earlier observation[25] the computed Δg_{XX} values for the models are significantly too large for most of the structures (even after scaling by 0.88 to account for systematic deficiencies of the DFT methods used) except for ones with two hydrogen bonds to the carbonyl and either none or one to the hydroxyl oxygen. However, the latter structures contradict the binding situation suggested by recent work of Yap *et al.*[18,24] who proposed a hydrogen bonding network with two hydrogen bond donors to the hydroxyl oxygen (O_1) and no additional hydrogen

bond to the carbonyl oxygen (O_4). In our calculations the values of Δg_{XX} remain nearly unchanged compared to the gas-phase value in all models that exhibit single-sided hydrogen bonding to the O_1 hydroxyl oxygen atom. The main redistribution of spin density from a nearly symmetric one in a semiquinone radical anion to a highly asymmetric one in a neutral semiquinone radical is due to the covalently bound hydrogen. Further hydrogen bonding to a hydroxyl oxygen affects the spin density distribution only a little resulting in nearly unchanged values of Δg_{XX}. However, addition of a hydrogen bond to a carbonyl oxygen results in an immediate lowering of Δg_{XX}, due to reduction of the spin–orbit (SO) contribution of this oxygen atom following the polarisation of spin density towards the *ipso* ring carbons. The scaled Δg_{XX} values of one-sided 2/0 hydrogen-bond (to the hydroxyl oxygen side) models are significantly larger than either experimental values or values computed for the most promising 2/1 hydrogen-bond models of semiquinone radical anion. In contrast, the asymmetric double-sided 2/1 model provides a Δg_{XX} value similar to those of 2/1 models of the semiquinone radical anion. The significant differences between these models are only evident after analysis of the computed hyperfine couplings with particular attention to ^{13}C hyperfine couplings (see below).

(iii) ^{13}C-Carbonyl hyperfine tensor

The significantly different A_{zz} components of the carbonyl ^{13}C hyperfine tensors for the C_1 and C_4 positions, and in particular the low value for the C_4 position, led one of us to initially favour a single-sided semiquinone radical anion hydrogen bonding model based on comparisons with model compound data.[17] As the above results for the g-tensors provide no strong indication for either neutral or anionic models, it is of great interest to evaluate the compatibility of the hyperfine tensors for different models with experimental observations. In ref. 25 we have shown that the differences between the ^{13}C hyperfine couplings of the carbonyl groups reflect specifically the asymmetry of the hydrogen-bonding framework, if one keeps in mind that one may not straightforwardly transfer HFC values from symmetrical to asymmetrical environments. We have also shown that single-sided hydrogen bonding in an anionic model would cause even larger differences between the two carbonyl sites than observed experimentally and in particular an even lower A_{ZZ} for the C_4 position.[25] In contrast, unsymmetrical double-sided anionic models, especially 2/1 models, provide much better agreement with the measured data for the Q_H site (see Table 4). Recently it has been suggested that exact measurements of the complete ^{13}C hyperfine tensors for C_1 and C_4 could unambiguously resolve between an anionic and a neutral form of semiquinone radicals.[27]

In Table 4 the computed ^{13}C hyperfine coupling tensors for all the models of a neutral protonated semiquinone radical are shown, in comparison with experimental data for a variety of environments as well as with our earlier data for anionic semiquinone models.[25] The differences between the C_1 and C_4 ^{13}C hyperfine couplings in all of the considered models are a few times larger than the experimentally found one and even than the one computed for single-sided models of semiquinone radical anion. Large positive values are computed for carbons neighbouring the hydroxyl group, while smaller but negative values are obtained for the carbonyl carbons, overall resulting in differences of about 70 to 90 MHz. Only small changes are observed while going from an isolated semiquinone radical to hydrogen-bonded models. These obvious results together with the experimental data would argue against a neutral semiquinone radical being stabilised in the Q_H binding site of QOX. Earlier resolved W-band EPR measurements using ^{13}C labelled quinones not only clearly resolved the A_{ZZ} values of the ^{13}C hyperfine tensor but also provided, through spectral simulations, upper limits for the A_{XX} and A_{YY} values.[17] These values also agree with an anionic form and are much lower than those calculated for a neutral species.

Table 4 ^{13}C Hyperfine coupling tensors (in MHz) for the C_1 and C_4 carbon positions in ubisemiquinone radical models

Model[a]	^{13}C-HFC at C_1			^{13}C-HFC at C_4		
	A_{XX}	A_{YY}	A_{ZZ}	A_{XX}	A_{YY}	A_{ZZ}
Models for neutral ubisemiquinone radical with hydroxyl group at O_1 position						
0/0	3.3	2.2	69.7	−23.6	−28.8	−16.5
1/0-a 1HO	3.6	2.6	70.6	−23.8	−29.0	−17.8
1/0-b 1HO	3.5	2.4	73.4	−23.9	−29.1	−17.8
1/0-c 1HO	2.7	1.6	69.9	−22.9	−28.0	−14.7
1/1 1HO-4HO	2.6	1.6	72.9	−21.9	−26.4	−18.2
0/2-a 4HO-4HO	1.6	2.6	78.4	−21.7	−25.1	−5.1
0/2-b 4HO-4HO	0.2	1.2	81.1	−24.1	−20.4	−4.0
1/2-a 1HO–4HO–4HO	−0.1	0.9	82.8	−23.5	−19.9	−4.2
1/2-b 1HO-4HO-4HO	1.5	2.4	84.6	−25.2	−21.3	−7.4
1/2-c 1HO-4HO-4HO	1.6	2.5	85.6	−25.0	−21.2	−7.7
2/0-a 1HO-1HO	4.5	3.6	74.5	−23.7	−28.8	−18.2
2/0-b 1HO-1HO	4.2	3.4	74.2	−23.6	−28.8	−17.6
2/0-c 1HO-1HO	2.9	1.8	70.5	−23.1	−28.2	−15.6
2/1 1HO-1HO-4HO	1.6	0.6	65.8	−21.3	−25.6	−2.7
Models for neutral ubisemiquinone radical with hydroxyl group at O_4 position						
0/0						
1/0-a 1HO	−26.3	−21.8	−5.1	1.2	2.2	67.5
1/0-b 1HO	−28.1	−23.4	−15.1	2.9	3.9	78.4
2/0 1HO-1HN	−24.8	−20.9	−2.4	1.4	2.4	78.9
Models for ubisemiquinone radical anion from ref. 25						
2/1-a 1HO–1HN–4HO	−11.2	−14.0	27.9	−12.0	−15.0	20.8
2/1-b 1HO–1HN–4HO	−11.1	−13.9	26.1	−12.6	−15.7	20.8
2/1-c 1HO–1HN–4HO	−11.0	−13.8	26.7	−13.1	−16.4	18.5
2/1-d 1HO–1HN–4HO	−10.8	−13.4	27.9	−13.5	−16.7	18.5
Experimental data						
Model[a]	^{13}C-HFC at C_1			^{13}C-HFC at C_4		
	A_{XX}	A_{YY}	A_{ZZ}	A_{XX}	A_{YY}	A_{ZZ}
$Q_H^{\bullet-}$ in bo_3-QOX [b]	*−4.2 (14)*	*−12.6 (14)*	*30.8 (8)*	*−7.0 (14)*	*−10.4 (14)*	*20.2 (8)*
$Q_A^{\bullet-}$ in Zn-bRCs[c]	−12.6(17)	−14.6(17)	22.7 (6)	−9.2 (17)	−9.8 (17)	35.0 (6)
$Q_A^{\bullet-}$ in Zn-bRCs[d]	15.4 (14)	18.2 (14)	22.4 (8)	<7.0 (14)	<7.0 (14)	35.6 (8)
$Q_B^{\bullet-}$ in Zn-bRCs[c]	−10.9 (17)	−13.2 (17)	27.7 (6)	−10.1 (17)	−10.4 (17)	32.2 (6)
UQ-3$^{\bullet-}$ in *i*PrOH[c]	−12.1 (17)	−10.4 (17)	30.6 (6)	−11.2 (17)	−9.8 (17)	32.2 (6)
UQ-10$^{\bullet-}$ in *i*PrOH[d]	n.d.	n.d.	31.7 (8)	n.d.	n.d.	30.8 (8)
UQ-3$^{\bullet-}$ in DME/MTHF[e]	−12.1 (22)	−15.1 (22)	20.5 (6)	−13.2 (22)	−15.4 (22)	20.5 (6)

[a] *cf.* Fig. 8. [b] Native UQ-8 substituted with ^{13}C selectively labelled UQ-2.[17] [c] Native UQ-10 substituted with selectively ^{13}C labelled UQ-3 (*cf.* ref. 94). [d] With selectively ^{13}C-labelled UQ-10.[95] [e] Ref. 91.

(iv) $^1H(CH_3)$-Hyperfine tensors

Table 5 shows the ^1H HFC tensors of the methyl group in the C_5-position, averaged over all three hydrogen atoms. For all the models with the hydroxyl group on the O_4 side, the computed values of the tensors are so small that we can ultimately neglect these structures and focus our discussion solely on the models with the hydroxyl

Table 5 5-Methyl ^{1}H hyperfine coupling tensors HFC (in MHz)[a]

Model[b]	^{1}H-HFC		
	A_{XX}	A_{YY}	A_{ZZ}
Models for neutral ubisemiquinone radical with hydroxyl group at O_1 position			
0/0	11.9	16.7	11.0
1/0-a 1HO	12.1	16.9	11.2
1/0-b 1HO	12.2	16.9	11.3
1/0-c 1HO	11.7	16.5	10.8
1/1 1HO-4HO	11.9	16.2	10.9
0/2-a 4HO-4HO	14.6	19.2	13.7
0/2-b 4HO-4HO	15.3	19.8	14.5
1/2-a 1HO-4HO-4HO	17.0	21.8	16.1
1/2-b 1HO-4HO-4HO	15.4	21.0	16.3
1/2-c 1HO-4HO-4HO	17.9	22.7	17.1
2/0-a 1HO-1HO	10.8	15.5	9.9
2/0-b 1HO-1HO	10.6	15.3	9.8
2/0-c 1HO-1HO	10.7	15.3	9.8
2/1 1HO-1HO-4HO	8.7	13.2	7.9
Models for neutral ubisemiquinone radical with hydroxyl group at O_4 position			
0/0			
1/0-a 1HO	−1.2	1.4	−1.9
1/0-b 1HO	−3.3	−0.6	−4.0
2/0 1HO-1HN	−3.3	−0.6	−4.0
Models for ubisemiquinone radical anion from ref. 25			
2/1-a 1HO-1HN-4HO	5.9	9.5	5.1
2/1-b 1HO-1HN-4HO	5.1	8.6	4.2
2/1-c 1HO-1HN-4HO	5.2	8.8	4.3
2/1-d 1HO-1HN-4HO	5.3	8.8	4.4
2/1 1HN-1HN-4HN	6.0	9.7	5.2
Experimental data			
$Q_H^{\cdot-}$ in bo_3-QOX[c]	*8.40*	*12.78*	*7.85*
$UQ_2^{\cdot-}$ in bo_3-QOX[d]	*8.3*	*12.6*	*8.3*
DDQ$^{\cdot-}$ in bo_3-QOX; (5-methyl)[d]	*8.4*	*12.5*	*8.4*
DDQ$^{\cdot-}$ in bo_3-QOX; (6-methyl)[d]	*2.0*	*4.9*	*2.0*
$Q_A^{\cdot-}$ in Zn-bRCs[e]	3.8 (1)	6.9(1)	3.2 (1)
$Q_B^{\cdot-}$ in Zn-bRCs[e]	4.4 (1)	7.8 (1)	3.9 (1)
DDQ$^{\cdot-}$ in *i*PrOH[d]	5.3 (3)	8.0 (3)	5.3 (3)
UQ-0$^{\cdot-}$ in *i*PrOH[f]	4.8 (3)	9.0 (3)	4.8 (3)
UQ-3$^{\cdot-}$ in *i*PrOH[f]	5.3 (3)	8.4 (3)	5.0 (3)
exp. UQ-10$^{\cdot-}$ in *i*PrOH[g]	4.8	8.5	4.8
UQ-0$^{\cdot-}$ in DME/mTHF[f]	5.0 (3)	8.4 (3)	5.0 (3)
UQ-3$^{\cdot-}$ in DME/mTHF[f]	5.0 (3)	8.1 (3)	5.0 (3)
UQ-10$^{\cdot-}$ in DME/mTHF[d]	5.2 (3)	8.4 (3)	5.2 (3)
$A^{\cdot-}$ in PS–I[h]	9.0	12.6	9.0
$A_1^{\cdot-}$ in PS I[i]	8.9(1)	12.5(1)	8.9(1)
calc. $VK_1^{\cdot-}$[j]	9.2	12.6	8.2

[a] *cf.* Fig. 1c for atom labels. Average HFC's for the three hydrogen atoms. [b] *cf.* Fig. 8. [c] Ref. 16. [d] This work. [e] Ref. 26. [f] X-band ENDOR and X- and Q-band EPR simulations.[91] [g] Ref. 41 [h] Ref. 96. [i] Ref. 97. [j] Ref. 67.

Table 6 ^{1}H hyperfine couplings (in MHz) for exchangeable hydrogen positions[a]

Model[b]	H-bond[b]	^{1}H-HFC/MHz			
		A_{iso}	A_{11}	A_{22}	A_{33}
Models for neutral ubisemiquinone radical with hydroxyl group at O_1 position					
0/0		−5.2	−10.1	−9.0	3.5
1/0-a 1HO		−4.8	−9.5	−8.5	3.7
	1HO	0.0	−0.6 (−0.8)[c]	−0.5 (−0.5)	1.1 (1.4)
1/0-b 1HO		−5.0	−9.9	−8.8	3.6
	1HO	0.1	−1.1	−1.0	2.5
1/0-c 1HO		−5.0	−10.8	−8.9	4.6
1/1 1HO–4HO		−5.0	−10.5	−9.3	3.8
	1HO	0.1	−1.1	−1.1	2.5
	4HO	0.1	−4.0	−3.7	8.1
0/2-a 4HO–4HO		−6.3	−12.5	−10.6	4.2
	4HO	−1.4	−5.9	−5.4	7.1
	4HO	−0.6	−3.7	−3.6	5.4
0/2-b 4HO–4HO		−7.3	−13.9	−12.2	4.2
	4HO	−1.3	−5.7	−5.3	7.0
	4HO	−0.6	−3.4	−3.4	5.11
0/1-a 1HO–4HO–4HO		−6.9	−14.9	−11.7	5.8
	4HO	−1.1	−5.1	−4.8	6.7
	4HO	−0.7	−3.4	−3.2	4.7
0/1-b 1HO–4HO–4HO		−6.6	−12.6	−11.2	4.1
	1HO	0.1	−1.3	−1.2	2.8
	4HO	−1.0	−5.2	−4.8	7.0
	4HO	−0.6	−3.4	−3.3	5.0
0/1-c 1HO–4HO–4HO		−6.9	−13.6	−11.4	4.4
	1HO	0	−1.2	−1.0	2.3
	4HO	−1.4	−5.7	−5.4	6.9
	4HO	−0.6	−3.5	−3.3	5.0
2/0-a 1HO–1HO		29.8	24.5	26.2	38.7
	1HO	0	−1.2	−0.4	1.5
	1HO	−0.1	−1.1	−0.8	1.4
2/0-b 1HO–1HO		26.2	20.9	22.4	35.4
	1HO	−0.2	−1.2	−0.8	1.4
	1HO	0	−1.3	−0.5	1.7
2/0-c 1HO–1HO		−5.0	−10.4	−8.5	4.0
	1HO	−0.2	−1.9	−1.7	2.9
	1HO	0	−0.7	−0.6	1.4
2/1 1HO–1HO–4HO		−5.0	−10.5	−8.6	4.0
	1HO	−0.2	−1.9	−1.7	2.8
	4HO	−1.8	−7.2	−7.0	8.9
Models for neutral ubisemiquinone radical with hydroxyl group at O_4 position					
0/0		−5.4	−10.4	−9.2	3.4
1/0-a 1HO		−5.4	−10.4	−9.3	3.4
	1HO	0.4	−3.5	−3.1	7.8
1/0-b 1HO		−5.5	−10.7	−9.5	3.7
	1HO	0.3	−3.5	−3.2	7.6
2/0 1HO–1HN		−6.4	−12.6	−10.8	4.1
	1HO	0.1	−3.3	−3.1	7.1
	1HN	−0.4	−3.9	−3.4	6.2
Models for ubisemiquinone radical anion from ref. 25					
2/1-a 1HO-1HN-4HO	1HO		−3.4	−3.1	6.3
	1HN		−2.5	−2.4	5.4
	4HO		−4.3	−4.1	6.7
2/1-b 1HO-1HN-4HO	1HO		−3.4	−3.1	6.3

Table 6 (*Contd.*)

Model[b]	H-bond[b]	^{1}H-HFC/MHz			
		A_{iso}	A_{11}	A_{22}	A_{33}
	1HN		−2.5	−2.4	5.2
	4HO		−4.4	−4.2	6.9
2/1-c 1HO-1HN-4HO	1HO		−3.3	−2.9	6.2
	1HN		−2.5	−2.4	5.3
	4HO		−4.4	−4.2	6.8
2/1-d 1HO-1HN-4HO	1HO		−4.1	−3.9	6.5
	1HN		−3.0	−2.8	5.5
	4HO		−5.0	−4.9	7.1
	Experimental data				
Q_H *in bo*$_3$-*QOX*[d]	HO	±0.7	±7.0	±7.0	∓11.9
Q_H *in bo*$_3$-*QOX*[d]	HO	∓1.2	∓5.4	5.4	±7.2
Q_H *in bo*$_3$-*QOX*[d]	HO	∓4.6	∓6.3	∓6.3	∓1.2
UQ-10$^{\cdot-}$ in iPrOH[e]	HO	+1.11	−1.33	−1.33	6.00
BQ$^{\cdot-}$ in iPrOH[f]	HO	+0.1	−2.8	−2.8	5.9
BQ$^{\cdot-}$ in H_2O[g]	HO		−2.66	−2.67	6.36
$Q_A^{\cdot-}$ in Zn-bRCc[h]	HN		(−)4.6	(−)4.6	8.9
Deuterated 2–methyl–NQ in PS–I[i]	HN		−4.9	−4.9	7.7

[a] HFC's of the covalently-bonded hydrogens are given in the first line for each model of a neutral semiquinone radical. [b] *cf.* Fig. 8. [c] Values given in brackets are for the hydrogen H-bonded to the methoxy-oxygen. [d] Ref. 24. [e] From ENDOR difference spectra (protonated minus deuterated 2-propanol).[41] [f] Ref.98. [g] Ref. 99. [h] Ref. 26. [i] Ref. 100.

group on the O_1 side. For all models but 2/1, all the tensor components (and thus the isotropic value) are 2–10 MHz too high relative to the observed experimental value. An outstanding agreement is found for 2/1 model for which the deviation of computed and experimental values is smaller than 0.5 MHz. However, one has to treat this agreement with care as previous studies[25] have shown that errors of a few MHz are to be expected even for realistic models. It appears that the ^{1}H(CH_3) couplings are generally more sensitive to small (unsymmetrical) changes in the wider environment of the semiquinone than, *e.g.*, ^{13}C HFC's or *g*-tensors. For example, the experimental ^{1}H(CH_3) HFC's for the Q_H site shown in Table 4 are measured at a pH of 6 but increase by about 2 MHz (see Fig. 5) upon changing to pH 8 (for all components). Keeping in mind the results computed for other binding sites and other model complexes,[25] we do not think that the ^{1}H(CH_3) HFC's can be used as a strong evidence for or against a model of a neutral semiquinone radical.

(v) ^{1}H-Hyperfine tensors for hydrogen-bonded protons

Table 6 provides ^{1}H HFC's for the hydrogen-bonded protons for models of a neutral semiquinone radical in comparison with experimental data for a variety of environments as well as with data from ref. 26 computed for our best models of semiquinone radical anion in the Q_H site.

Again in the recent work of Yap *et al.*[24] the authors suggest hyperfine coupling constants for up to three exchangeable protons, two of which should be hydrogen-bonded to the radical, and the third one is assigned to a hydrogen atom

Table 7 Computed ^{17}O hyperfine coupling tensors HFC (in MHz) for the O_1 and O_4 positions

Model[a]	^{17}O-HFC at O_1			^{17}O-HFC at O_4		
	A_{XX}	A_{YY}	A_{ZZ}	A_{XX}	A_{YY}	A_{ZZ}
Models for neutral ubisemiquinone radical with hydroxyl group at O_1 position						
0/0	5.2	4.4	−34.4	30.8	30.3	−133.8
1/0-a 1HO	5.0	4.1	−34.0	30.8	30.4	−133.6
1/0-b 1HO	5.0	4.1	−33.4	31.1	30.6	−134.3
1/0-c 1HO	5.5	4.7	−37.9	30.0	29.6	−131.3
1/1 1HO-4HO	5.3	4.4	−35.9	26.9	26.4	−125.4
0/2-a 4HO-4HO	6.3	5.3	−40.9	25.4	25.0	−116.4
0/2-b 4HO-4HO	7.2	6.2	−46.5	24.0	23.6	−111.1
1/2-a 1HO-4HO-4HO	7.7	6.6	−49.8	23.1	22.7	−107.7
1/2-b 1HO-4HO-4HO	6.4	5.5	−42.9	24.8	24.4	−114.0
1/2-c 1HO-4HO-4HO	6.8	5.7	−43.3	24.5	24.2	−112.7
2/0-a 1HO–1HO	−5.3	−4.5	−31.22	30.6	30.1	−132.74
2/0-b 1HO–1HO	−3.6	−4.3	−32.2	30.5	30.0	−132.6
2/0-c 1HO-1HO	5.2	4.3	−36.0	30.2	29.8	−131.7
2/1 1HO-1HO-4HO	5.3	4.4	−36.4	26.2	25.7	−124.6
Models for neutral ubisemiquinone radical with hydroxyl group at O_4 position						
0/0						
1/0-a 1HO	27.0	26.4	−127.5	5.4	4.6	−35.0
1/0-b 1HO	26.7	26.3	−121.8	5.5	4.5	−36.0
2/0 1HO-1HN	24.1	23.7	−115.4	6.4	5.4	−41.0
Models for ubisemiquinone radical anion from ref. 1						
2/1-a 1HO-1HN-4HO	16.3	15.5	−88.2	17.8	17.1	−91.2
2/1-b 1HO–1HN–4HO	15.5	14.8	−87.4	18.3	17.6	−94.6
2/1-c 1HO–1HN–4HO	15.6	14.8	−87.6	18.4	17.7	−95.4
2/1-d 1HO–1HN–4HO	15.1	14.4	−85.5	18.5	17.9	−95.6
Experimental data						
$Q_A^{\cdot-}$ in Zn-bRC$_m$[b]			(−)94			(−)75
$Q_B^{\cdot-}$ in Zn-bRC$_m$[b]			(−)88			(−)82
$BQ^{\cdot-}$ in *i*PrOH[c]			−91.6			−91.6
$DQ^{\cdot-}$ in *i*PrOH[d]			−81.4			−81.4
2-methyl-NQ in *i*PrOH[e]			(−)78			n.d.
2-methyl-NQ in PS I[f]	4.5	4.5	(−)77	4.5	4.5	(−)84
calc. $VK_1^{\cdot-}$ [g]	13.4	14.0	−83.1	19.6	20.1	−97.3

[a] *cf.* Fig. 8. [b] *cf.* Ref. 26. [c] From W-band EPR in frozen deuterated 2-propanol[41] [d] From Q-band EPR in frozen deuterated 2-propanol [41] [e] Ref.101. [f] Ref. 102. [g] B3LYP/EPR-II calculations on an A_1 model made from vitamin K_1 and a methyl-imidazole molecule H-bonded to O_4.[67]

covalently bound to O_1. The covalently bound proton would then possess a large anisotropic hyperfine coupling ($A_\perp = \pm 7.0$ MHz, $A_\parallel = \mp 11.9$ MHz; see Table 6) with a very small isotropic contribution ($a = \pm 0.7$ MHz). The covalent character is deduced based on the point-dipole approximation which for such a large dipolar coupling $|T| = \mp 6.3$ MHz ($A_\perp = a - T$; $A_\parallel = a + 2T$) would impose an O − H distance of the order of 1.2 Å. In contradiction to these experimental results, in all our models (except 2/0-a and –b) the covalently bound hydrogen exhibits an isotropic hyperfine coupling of 4–5 MHz. Extreme values of 29.8 and 26.2 MHz computed for the 2/0–a and –b structures, respectively, are due to the large

out-of-plane geometry of the covalently bonded hydrogen. However, hyperfine coupling constants similar to the experimental values were calculated for the hydrogen H-bonded to the O_4 carbonyl oxygen in the 2/1 model where the isotropic contribution is only –1.8 MHz and the anisotropic components are large ($A_\perp$ = –7.0(−7.2) MHz and $A_\parallel$ = 8.9 MHz). Large anisotropic components of the hyperfine coupling tensor are due to the strong out-of-plane geometry of the hydrogen bond withγ equal to 60° (Table 2). One of the exchangeable protons observed experimentally[24] possesses such a large anisotropic hyperfine splitting. The authors suggest that this proton (i) might be the second proton of the $–NH_2$ group not participating in an H-bond with the semiquinone radical, (ii) could form an H-bond to the oxygen of a methoxy group, or (iii) could be a proton at a second shell distance. None of these suggestions explains the large spin density transferred to this proton and indeed it may be prudent to speculate about the interpretation of the experimental data in ref. 24. For our neutral semiquinone models an isotropic contribution of 5–7 MHz was calculated for the covalently bound hydrogens (except for the even larger values of the 2/0 models with strong out-of-plane geometry of covalently bound hydrogen). The large dipolar contributions, however, provide major discrepancies to the experimental values. Nevertheless, the computed hyperfine couplings show that the covalently bound hydrogen in a neutral semiquinone should possess a relatively large isotropic as well as dipolar contribution to the hyperfine coupling tensor, which is not observed experimentally.

(vi) ^{17}O-Hyperfine tensors

No ^{17}O carbonyl hyperfine couplings have as yet been measured for semiquinones in QOX although such experiments have been performed on the semiquinones in the bacterial reaction centres.[26] Table 7 provides the predicted values for the different anionic and neutral supermolecular model complexes. For the 2/1 double-sided model of semiquinone radical anion, the difference between the O_1- and O_4-positions was only about 1.5–2.0 MHz for all three components, with the value of O_1 being lower. Larger differences were observed for other models.[25] For models of the neutral semiquinone radical a difference of about 60 to 100 MHz is found for A_{ZZ} (with the value for the carbonyl oxygen being smaller), whereas the A_{XX} and A_{YY} components are about 16 to 26 MHz larger at the carbonyl oxygen. The possible measurement of these parameters would provide further unambiguous proof for the nature of the semiquinone radical in QOX, and such experiments are planned in the laboratory of one of the authors.

Conclusions

In summary we have used both advanced spectroscopic techniques and modern quantum chemical calculations to study both the electronic nature of the semiquinone formed at the Q_H binding site of the cytochrome *bo*$_3$ ubiquinol oxidase (QOX) from *Escherichia coli* (*E. coli*) and also its specific binding to the protein. This membrane protein is a transmembrane protein belonging to the family of terminal copper-heme oxidases of the aerobic respiratory chain and acts as a redox-driven proton pump that couples the vectorial translocation of protons across the membrane to the reduction of molecular oxygen to water. Here we demonstrate the complementarities of both X-ray crystallography and modern advanced biophysical spectroscopy combined with quantum-chemical theory. The successful structure determination of a membrane protein, especially of this important class of enzymes, was a huge challenge, however there still remains several important issues *e.g.* the nature/position and function of one of its cofactors that require the use of such complementary techniques. At the same time the correlation of structure with spectroscopic data is also a challenge which, as we show here, is only really possible through application of modern quantum chemical calculations.

We have identified, as have others, the nature of the ligand to which Q_H binds in its paramagnetic form.[16–18,24] Through use of $^{14}N/^{15}N$ isotope labelling we are, however, able to give an accurate distance determination between Q_H and its binding ligand. There are, however, pitfalls in such analysis as we clearly point out, which can lead to mistaken analysis (in this case of a mono-protonated neutral radical). The use of two-dimensional correlation techniques, while maybe seeming to be overkill, does indeed substantially support our analysis and we are sure there are many cases in the literature that could benefit from such attention to detail. Indeed we hope we have shown that such "complex" techniques have their merits. The use of site-directed variants was used to further identify and characterise this binding pocket, and initially the results we obtained in 2001[16] led to a partially mistaken interpretation. This was based on using existing published data rather than being prepared to think of the as yet unobserved. There are now a couple of examples of semiquinones binding, not only to histidine,[71,74] tryptophan[82] and peptide nitrogen[72] but also to arginine (*e.g.* the bc_1 complex[83] and possibly in PQQ[84]). The use of site-directed mutagenesis again still provides conflicting results as the introduction of a second histidine into the binding pocket has resulted in the detection of such an interaction. The question remains, however, which one? Here we demonstrate that through careful selection of replacement molecules and comparison with *in vitro* experiments this question could be answered. From the evidence presented here it seems quite clear that in D75H variant H98 is now directly coordinating Q_H resulting in loss of enzymatic activity. Debates about the direct coordination of histidine to semiquinones are currently occurring in other quinone containing proteins *e.g.* in the bc_1 complex[85,86] where the presence of an intermediate bound water molecule may explain the observed spectroscopic differences. Such a bound water molecule may also occur between Q_H and His98 in WT QOX, aiding its function, while in the H98F variant a complete loss of enzymatic activity[21] is observed, which may correlate with the absence of such a bound water molecule.

Further, the quantum chemical calculations presented here demonstrate how detailed we can now be when comparing experimental data, and indeed the overall agreement between theory and experiment is quite impressive, to the point that the existing suggestion of a mono-protonated neutral radical can be categorically ruled out. There are still several important quinone binding proteins, involved in important bioenergetic processes, *e.g.* the cytochrome bc_1 complex, where semiquinones have still to be identified and characterised in such detail as to permit important functional discussion.[87,88] We hope that this example will motivate such detailed experimentation in these and other systems in the future.

Acknowledgements

Fraser MacMillan is a Wolfson Merit Award holder of the Royal Society which is gratefully acknowledged for its financial support. This work has also been supported by the Deutsche Forschungsgemeinschaft (SFB 472). We are grateful to Monique van Straaten for excellent technical assistance and to Dr Stéphane Grimaldi (now University Marseille, France) who was very actively involved in some of the initial experiments which were performed in the laboratory of Prof. T. F. Prisner (J. W. Goethe University, Frankfurt, Germany) who is also gratefully acknowledged for access to his pulsed EPR instrumentation. We are indebted to Prof. R. B. Gennis (University of Illinois, Urbana-Champaign, USA) for ongoing discussion. Dr Friedhelm Lendzian (Technische Universität Berlin, Berlin, Germany) is acknowledged for his help with the electrochemical generation of semiquinones and for many years of active discussion and support.

References

1 M. W. Calhoun, J. W. Thomas and R. B. Gennis, *Trends Biochem. Sci.*, 1994, **19**, 325–330.
2 J. A. Garciahorsman, B. Barquera, J. Rumbley, J. X. Ma and R. B. Gennis, *J. Bacteriol.*, 1994, **176**, 5587–5600.

3 T. T. Mogi, Motonari, Hiroshi Hori, Hideto Miyoshi, Haruki Nakamura and Yasuhiro Anraku, *J. Biochem., Mol. Biol. Biophys.*, 1998, **2**, 79–110.
4 M. Sato-Watanabe, T. Mogi, T. Ogura, T. Kitagawa, H. Miyoshi, H. Iwamura and Y. Anraku, *J. Biol. Chem.*, 1994, **269**, 28908–28912.
5 M. Sato-Watanabe, T. Mogi, H. Miyoshi and Y. Anraku, *Biochemistry*, 1998, **37**, 5356–5361.
6 M. Sato-Watanabe, T. Mogi, K. Sakamoto, H. Miyoshi and Y. Anraku, *Biochemistry*, 1998, **37**, 12744–12752.
7 J. X. Ma, A. Puustinen, M. Wikstrom and R. B. Gennis, *Biochemistry*, 1998, **37**, 11806–11811.
8 P. H. Tsatsos, K. Reynolds, E. F. Nickels, D. Y. He, C. A. Yu and R. B. Gennis, *Biochemistry*, 1998, **37**, 9884–9888.
9 K. Sakamoto, T. Mogi, S. Noguchi and N. Sone, *Journal of Biochemistry - Tokyo*, 1999, **126**, 934–939.
10 M. Sato-Watanabe, S. Itoh, T. Mogi, K. Matsuura, H. Miyoshi and Y. Anraku, *FEBS Lett.*, 1995, **374**, 265–269.
11 W. J. Ingledew, T. Ohnishi and J. C. Salerno, *Eur. J. Biochem.*, 1995, **227**, 903–908.
12 J. P. M. Osborne, S. M. Schultz, B. E. Edmondson, D. E. Chan, S. I., and R. B. Gennis., in *Oxygen Homeostasis and Its Dynamics*, ed. Y. Ishimura, Shimada, H., and Suematsu, M., Springer-Verlag, Tokyo, 1998, pp. 33–39.
13 B. E. Schultz, D. E. Edmondson and S. I. Chan, *Biochemistry*, 1998, **37**, 4160–4168.
14 A. V. Veselov, J. P. Osborne, R. B. Gennis and C. P. Scholes, *Biochemistry*, 2000, **39**, 3169–3175.
15 S. F. Hastings, P. Heathcote, W. J. Ingledew and S. E. Rigby, *Eur. J. Biochem.*, 2000, **267**, 5638–5645.
16 S. Grimaldi, F. MacMillan, T. Ostermann, B. Ludwig, H. Michel and T. Prisner, *Biochemistry*, 2001, **40**, 1037–1043.
17 S. Grimaldi, T. Ostermann, N. Weiden, T. Mogi, H. Miyoshi, B. Ludwig, H. Michel, T. F. Prisner and F. MacMillan, *Biochemistry*, 2003, **42**, 5632–5639.
18 L. L. Yap, R. I. Samoilova, R. B. Gennis and S. A. Dikanov, *J. Biol. Chem.*, 2007, **282**, 8777–8785.
19 J. Abramson, S. Riistama, G. Larsson, A. Jasaitis, M. Svensson-Ek, L. Laakkonen, A. Puustinen, S. Iwata and M. Wikstrom, *Nat. Struct. Biol.*, 2000, **7**, 910–917.
20 C. Ostermeier, A. Harrenga, U. Ermler and H. Michel, *Proc. Natl. Acad. Sci. U. S. A.*, 1997, **94**, 10547–10553.
21 P. Hellwig, T. Yano, T. Ohnishi and R. B. Gennis, *Biochemistry*, 2002, **41**, 10675–10679.
22 P. Hellwig, B. Barquera and R. B. Gennis, *Biochemistry*, 2001, **40**, 1077–1082.
23 M. T. Lin, Rimma I. Samoilova, R. B. Gennis and S. A. Dikanov, *J. Am. Chem. Soc.*, 2008, **130**(47), 15768–15769.
24 L. L. Yap, R. I. Samoilova, R. B. Gennis and S. A. Dikanov, *J. Biol. Chem.*, 2006, **281**, 16879–16887.
25 S. Kacprzak, M. Kaupp and F. MacMillan, *J. Am. Chem. Soc.*, 2006, **128**, 5659–5671.
26 W. Lubitz and G. Feher, *Appl. Magn. Reson.*, 1999, **17**, 1–48.
27 S. E. Boesch and R. A. Wheeler, *ChemPhysChem*, 2009, **10**(18), 3187–3189.
28 J. N. Rumbley, E. F. Nickels and R. B. Gennis, *Biochim. Biophys. Acta, Protein Struct. Mol. Enzymol.*, 1997, **1340**, 131–142.
29 T. Schroter, C. Winterstein, B. Ludwig and O. M. Richter, *FEBS Lett.*, 1998, **432**, 109–112.
30 L. J. Lemieux, M. W. Calhoun, J. W. Thomas, W. J. Ingledew and R. B. Gennis, *J. Biol. Chem.*, 1992, **267**, 2105–2113.
31 P. Hellwig, T. Mogi, F. L. Tomson, R. B. Gennis, J. Iwata, H. Miyoshi and W. Maentele, *Biochemistry*, 1999, **38**, 14683–14689.
32 F. Lendzian, M. Plato and K. Mobius, *J. Magn. Reson.*, 1981, **44**, 20–31.
33 R. P. J. Merks and R. De Beer, *J. Phys. Chem.*, 1979, **83**, 3319–3322.
34 W. B. Mims, *Phys. Rev. B: Solid State*, 1972, **6**, 3543.
35 P. Hofer, A. Grupp, H. Nebenfuhr and M. Mehring, *Chem. Phys. Lett.*, 1986, **132**, 279–282.
36 J. M. Fauth, A. Schweiger, L. Braunschweiler, J. Forrer and R. R. Ernst, *J. Magn. Reson.*, 1986, **66**, 74–85.
37 C. Gemperle, G. Aebli, A. Schweiger and R. R. Ernst, *J. Magn. Reson.*, 1990, **88**, 241–256.
38 D. Goldfarb, V. Kofman, J. Libman, A. Shanzer, R. Rahmatouline, S. Van Doorslaer and A. Schweiger, *J. Am. Chem. Soc.*, 1998, **120**, 7020–7029.
39 O. Burghaus, M. Plato, M. Rohrer, K. Möbius, F. MacMillan and W. Lubitz, *J. Phys. Chem.*, 1993, **97**, 7639–7647.
40 M. Rohrer, M. Plato, F. MacMillan, Y. Grishin, W. Lubitz and K. Möbius, *J. Magn. Reson.*, 1995, **116**, 59–66.

41 F. MacMillan, F. Lendzian and W. Lubitz, *Magn. Reson. Chem.*, 1995, **33**, S81–S93.
42 A. D. Becke, *Phys. Rev. A: At., Mol., Opt. Phys.*, 1988, **38**, 3098–3100.
43 J. P. Perdew and Y. Wang, *Phys. Rev. B: Condens. Matter*, 1986, **33**, 8822–8824.
44 N. Godbout, D. R. Salahub, J. Andzelm and E. Wimmer, *Can. J. Chem.*, 1992, **70**, 560–571.
45 K. Eichkorn, O. Treutler, H. Öhm, M. Häser and R. Ahlrichs, *Chem. Phys. Lett.*, 1995, **242**, 652–660.
46 R. Ahlrichs, M. Bär, M. Häser, H. Horn and C. Kölmel, *Chem. Phys. Lett.*, 1989, **162**, 165–169.
47 R. Ahlrichs and M. von Arnim, in *Methods and Techniques in Computational Chemistry*, ed. E. Clementi and G. Corongiu, Club Europeen MOTECC, 1995, p. 509.
48 O. L. Malkina, J. Vaara, B. Schimmelpfennig, M. Munzarova, V. G. Malkin and M. Kaupp, *J. Am. Chem. Soc.*, 2000, **122**, 9206–9218.
49 M. Kaupp, R. Reviakine, O. L. Malkina, A. Arbuznikov, B. Schimmelpfennig and V. G. Malkin, *J. Comput. Chem.*, 2002, **23**, 794–803.
50 M. Kaupp, in *Progress in Theoretical Chemistry and Physics*, ed. A. Lund and M. Shiotani, Kluwer, Dordrecht, 2003, pp. 267–302.
51 M. Kaupp, C. Remenyi, J. Vaara, O. L. Malkina and V. G. Malkin, *J. Am. Chem. Soc.*, 2002, **124**, 2709–2722.
52 V. G. Malkin, O. L. Malkina, R. Reviakine, A. V. Arbuznikov, M. Kaupp, B. Schimmelpfennig, I. Malkin, T. Helgaker and K. Ruud, 2003.
53 B. A. Hess, C. M. Marian, U. Wahlgren and O. Gropen, *Chem. Phys. Lett.*, 1996, **251**, 365–371.
54 B. Schimmelpfennig, PhD Thesis, Stockholms Universitet, Stockholm, Sweden, 1996.
55 A. D. Becke, *J. Chem. Phys.*, 1993, **98**, 5648–5652.
56 C. Lee, W. Yang and R. G. Parr, *Phys. Rev. B: Condens. Matter*, 1988, **37**, 785–789.
57 B. Miehlich, A. Savin, H. Stoll and H. Preuss, *Chem. Phys. Lett.*, 1989, **157**, 200–206.
58 A. V. Arbuznikov and M. Kaupp, *Chem. Phys. Lett.*, 2004, **391**, 16–21.
59 A. V. Arbuznikov and M. Kaupp, *Chem. Phys. Lett.*, 2004, **386**, 8–16.
60 V. Barone, in *Recent Advances in Density Functional Methods*, ed. D. P. Chong, World Scientific Publ. Co., Singapore, 1996.
61 H. L. Flanagan and D. J. Singel, *J. Chem. Phys.*, 1987, **87**, 5606–5616.
62 J. J. Shane, P. Hofer, E. J. Reijerse and E. Deboer, *J. Magn. Reson.*, 1992, **99**, 596–604.
63 G. Jeschke, R. Rakhmatullin and A. Schweiger, *J. Magn. Reson.*, 1998, **131**, 261–271.
64 E. R. Davies, *Phys. Lett. A*, 1974, **47**, 1–2.
65 H. M. McConnell, *J. Chem. Phys.*, 1956, **24**, 764–766.
66 M. Sato-Watanabe, T. Mogi, H. Miyoshi, H. Iwamura, K. Matsushita, O. Adachi and Y. Anraku, *J. Biol. Chem.*, 1994, **269**, 28899–28907.
67 P. J. O'Malley, *Biochim. Biophys. Acta, Bioenerg.*, 1999, **1411**, 101–113.
68 J. Boiden Pedersen, C. E. M. Hansen, H. Parbo and L. T. Muus, *J. Chem. Phys.*, 1975, **63**, 2398–2405.
69 D. T. Edmonds, *Phys. Rep.*, 1977, **29**, 233–290.
70 R. Blinc, M. Mali, R. Osredkar, J. Seliger and L. Ehrenber., *Chem. Phys. Lett.*, 1974, **28**, 158–159.
71 F. Lendzian, J. Rautter, H. Käβ, A. Gardiner and W. Lubitz, *Ber. Bunsen-Ges.*, 1996, **100**, 2036–2040.
72 Y. Deligiannakis, J. Hanley and A. W. Ruthesford, *J. Am. Chem. Soc.*, 1999, **121**, 7653–7664.
73 J. Fritscher, *Phys. Chem. Chem. Phys.*, 2004, **6**, 4950–4956.
74 A. P. Spoyalov, R. J. Hulsebosch, S. Shochat, P. Gast and A. J. Hoff, *Chem. Phys. Lett.*, 1996, **263**, 715–720.
75 N. Fisher and P. R. Rich, *J. Mol. Biol.*, 2000, **296**, 1153–1162.
76 I. A. Safin and Y. D. Osokin, "Yadernyj kvadrupol'nyj rezonans v soedineniyakh azota", "Nuclear Quadrupole Resonance in Compounds of Nitrogen", Moscow, 1977.
77 A. J. Hoff, *Advanced EPR: Applications in Biology and Biochemistry*, New York, NY, U.S.A.: Elsevier, 1989; A. J. Hoff, *Distributors for the U.S. and Canada*, Elsevier Science Pub. Co., Amsterdam; New York, 1989.
78 A. Lai, H. L. Flanagan and D. J. Singel, *J. Chem. Phys.*, 1988, **89**, 7161–7166.
79 W. B. Mims, *Proc. R. Soc. London, Ser. A*, 1965, **283**, 452.
80 S. Grimaldi, R. Arias-Cartin, P. Lanciano, S. Lyubenova, B. Endeward, T. F. Prisner, A. Magalon and B. Guigliarelli, *J. Biol. Chem.*, 2010, **285**, 179–187.
81 J. H. Freed, C. S. David, D. C. Shreffler and S. G. Nathenson, *J. Immunol.*, 1978, **121**, 91–97.
82 J. Hanley, Y. Deligiannakis, F. MacMillan, H. Bottin and A. W. Rutherford, *Biochemistry*, 1997, **36**, 11543–11549.

83 M. Bawn, J. W. Cooley and F. MacMillan, *to be published*, 2010.
84 C. W. M. Kay, B. Mennenga, H. Gorisch and R. Bittl, *Proc. Natl. Acad. Sci. U. S. A.*, 2006, **103**, 5267–5342.
85 F. MacMillan, C. Lange, M. Bawn and C. Hunte, Applied Magnetic Resonance, 37, pp. 305–316.
86 D. R. J. Kolling, R. I. Samoilova, J. T. Holland, E. A. Berry, S. A. Dikanov and A. R. Crofts, *J. Biol. Chem.*, 2003, **278**, 39747–39754.
87 J. L. Cape, M. K. Bowman and D. M. Kramer, *Proc. Natl. Acad. Sci. U. S. A.*, 2007, **104**, 7887–7892.
88 H. Zhang, A. Osyczka, P. L. Dutton and C. C. Moser, *Biochim. Biophys. Acta, Bioenerg.*, 2007, **1767**, 883–887.
89 D. T. Edmonds and C. P. Summers, *Journal of Magnetic Resonance*, 1973, **12**, 134–142.
90 R. A. Isaacson, F. Lendzian, E. C. Abresch, W. Lubitz and G. Feher, *Biophys. J.*, 1995, **69**, 311–322.
91 O. Nimz, F. Lendzian, C. Boullais and W. Lubitz, *Appl. Magn. Reson.*, 1998, **14**, 255–274.
92 S. G. Zech, W. Hofbauer, A. Kamlowski, P. Fromme, D. Stehlik, W. Lubitz and R. Bittl, *J. Phys. Chem. B*, 2000, **104**, 9728–9739.
93 F. MacMillan, J. Hanley, L. van der Weerd, M. Knüpling, S. Un and A. W. Rutherford, *Biochemistry*, 1997, **36**, 9297–9303.
94 R. A. Isaacson, E. C. Abresch, F. Lendzian, C. Boullais, M. L. Paddock, C. Mioskowski, W. Lubitz and G. Feher, in *The reaction center of photosynthetic bacteria, structure and dynamics*, ed. M.-E. Michael-Beyerle, Springer-Verlag, Berlin, Germany, 1996, pp 353–367.
95 J. S. van den Brink, A. P. Spoyalov, P. Gast, W. B. S. van Liemt, J. Raap, J. Lugtenburg and A. J. Hoff, *FEBS Lett.*, 1994, **353**, 273–276.
96 S. E. Rigby, M. C. Evans and P. Heathcote, *Biochemistry*, 1996, **35**, 6651–6656.
97 C. Teutloff, R. Bittl and W. Lubitz, *Appl. Magn. Reson.*, 2004, **26**, 5–21.
98 P. J. O'Malley and G. T. Babcock, *J. Am. Chem. Soc.*, 1986, **108**, 3995–4001.
99 M. Flores, R. A. Isaacson, R. Calvo, G. Feher and W. Lubitz, *Chem. Phys.*, 2003, **294**, 401–413.
100 Y. N. Pushkar, D. Stehlik, M. van Gastel and W. Lubitz, *J. Mol. Struct.*, 2004, **700**, 233–241.
101 F. MacMillan, C. Teutloff, C. Boullais and W. Lubitz, unpublished results.
102 Y. N. Pushkar, O. Ayzatulin and D. Stehlik, *Appl. Magn. Reson.*, 2005, **28**, 195–211.
103 W. B. Mims, K. Nassau and J. D. Mcgee, *Phys. Rev.*, 1961, **123**, 2059.
104 S. A. Dikanov, J. T. Holland, B. Endeward, D. R. Kolling, R. I. Samoilova, T. F. Prisner and A. R. Crofts, *J. Biol. Chem.*, 2007, **282**, 25831–25841.
105 J. M. Peloquin, X. S. Tang, B. A. Diner and R. D. Britt, *Biochemistry*, 1999, **38**, 2057–2067.
106 J. Fritscher, T. Prisner and F. MacMillan, *Appl. Magn. Reson.*, 2006, **30**, 251–268.

